Precambrian Research 377 (2022) 106725

Contents lists available at ScienceDirect

Precambrian Research

journal homepage: www.elsevier.com/locate/precamres

Where did the Kontum Massif in central Vietnam come from?

Wei Jiang [a], Jin-Hai Yu [a,b,*], W.L. Griffin [b], Fangqian Wang [a], Xiaolei Wang [a], TrungHieu Pham [c], DinhLuyen Nguyen [a,d]

[a] State Key Laboratory for Mineral Deposits Research, School of Earth Sciences and Engineering, Nanjing University, Nanjing 210046, China
[b] ARC Centre of Excellence for Core to Crust Fluid Systems, and GEMOC, Department of Earth and Planetary Sciences, Macquarie University, Sydney, N.S.W. 2109, Australia
[c] Faculty of Geology, University of Science Ho Chi Minh City, Ho Chi Minh, Viet Nam
[d] Ha Noi University of Mining and Geology, Ha Noi, Viet Nam

ARTICLE INFO

Keywords:
U-Pb-Hf isotope
Detrital zircon
Precambrian basement
Supercontinent
Kontum Massif
Indochina Block

ABSTRACT

The Kontum Massif (KTM) is the largest Precambrian basement exposure in the Indochina Block, Southeast Asia. The compositions and formation ages of the KTM basement rocks and the paleo-position of the KTM in Proterozoic supercontinents have not been well constrained. Zircon U-Pb-Hf isotopic data of sixteen samples from the KTM in this study indicate that the KTM basement consists mainly of different units of metasedimentary rocks. These sedimentary rocks were deposited in five periods, late Paleoproterozoic (G1, 1.80–1.65 Ga), late Paleoproterozoic - early Mesoproterozoic (G2, 1.74–1.45 Ga), Mesoproterozoic (G3, 1.4–1.1 Ga), late Mesoproterozoic - early Neoproterozoic (G4, 1.1–0.81 Ga), and late Neoproterozoic - early Paleozoic (G5, 0.61–0.51 Ga), and underwent three phases of metamorphism in the early Paleozoic (501–415 Ma), late Paleozoic (371–331 Ma), and Indosinian (272–235 Ma). The G1 and G2 sedimentary rocks have abundant Neoarchean (2.63–2.48 Ga) and late Paleoproterozoic (1.83–1.74 Ga) detritus, and the G3 and G4 sedimentary rocks consist mainly of late Paleoproterozoic (1.74–1.72 Ga) and middle Mesoproterozoic (1.41–1.35 Ga) clastic materials. The G5 sedimentary rocks are characterized by consecutive Mesoproterozoic detrital zircon age spectra with a wide age peak at 1.06–1.01 Ga, much different from the G1 to G4 sedimentary rocks. Most Archean detrital zircons show juvenile Hf isotopes, whereas late Paleoproterozoic, middle Mesoproterozoic, and Grenvillian zircons show large Hf-isotope variations. Most detrital zircons are exotic because coeval igneous rocks have not been identified in the KTM (or elsewhere in Indochina), except ~1.44 Ga ones.

Comprehensive comparisons of detrital zircon U-Pb, Hf isotopes and sedimentary environments of these five units of sedimentary rocks with the extensive magmatism and coeval siliciclastic rocks in different cratons and microcontinents suggest that most of the Precambrian sediments in the KTM were derived from southwestern Laurentia, and the KTM has maintained a long-time connection with southwestern Laurentia for about one billion years from the G1 to the G4. The KTM was adjacent to Hainan Island and Tasmania during the G3-G4 deposition. The U-Pb ages and Hf isotopes of detrital zircons and sedimentary environment of the G5 sedimentary rocks indicate that the KTM was located on the northern margin of East Gondwana and near South China, India and western Australia, consistent with previous configurations for the Indochina Block. Therefore, the KTM, together with South China and Hainan Island, experienced quick northward movement from southwestern Laurentia to the northern margin of East Gondwana during the G4 (ca 1.10–0.81 Ga) to the G5 (0.61–0.51 Ga), which is also supported by new paleomagnetic data.

1. Introduction

The dispersed continents have amalgamated into supercontinents several times during the Earth's history (Cawood et al., 2018), such as late Paleoproterozoic Columbia (or Nuna) and late Mesoproterozoic Rodinia. The assembly and disaggregation of supercontinents recorded complex processes of the Earth evolution. Therefore, supercontinent reconstruction has been a hot research topic. The configurations of Precambrian supercontinents have been continuously refined based on new petrologic and paleomagnetic data obtained from finite

* Corresponding author.
E-mail address: jhyu@nju.edu.cn (J.-H. Yu).

https://doi.org/10.1016/j.precamres.2022.106725
Received 25 March 2022; Received in revised form 7 May 2022; Accepted 9 May 2022
Available online 20 May 2022

Precambrian terranes. The Indochina Block, an important terrane in Southeast Asia, has been missing in the Columbia and Rodinia supercontinent configurations due to the deficiency of Precambrian research. The Kontum Massif (KTM), situated in central Vietnam, eastern Indochina Block (Fig. 1a), was traditionally regarded as an Archean metamorphic complex (Hutchison, 1989), mainly based on its petrologic similarity to the classical Archean granulite terranes in East Gondwana. Nevertheless, geochronological data indicate that the granulite-facies metamorphism in the KTM occurred in the early Paleozoic and Indosinian times (Nakano et al., 2013, 2021; Tran et al., 2014; Bui et al., 2020). Based on Sr-Nd isotopic data from these metamorphic rocks, Lan et al. (2003) argued against the presence of an extensive Archean basement, and proposed that the KTM basement is mainly composed of Proterozoic rocks. The compositions and exact formation ages of the protoliths of these metamorphic rocks in the KTM were poorly constrained. It is well known that the Indochina Block together with South China Block was located on the northern margin of East Gondwana in the late Neoproterozoic to early Paleozoic and drifted northward in the Devonian (Metcalfe, 2021). However, the affinities of the Indochina Block with other continents and its paleo-positions in the Columbia and Rodinia supercontinents are unclear. Recently, Wang et al. (2020) argued that the KTM comprises Mesoproterozoic igneous rocks and Precambrian sedimentary rocks with depositional ages ranging from the late Paleoproterozoic to late Neoproterozoic, overlapping the evolution of the Columbia and Rodinia supercontinents. Nakano et al. (2021) also identified Mesoproterozoic magmatic rocks and late Paleoproterozoic to early Mesoproterozoic and Neoproterozoic sedimentary rocks in the KTM. These rocks provide a possibility to connect the KTM or the Indochina Block with the Columbia and Rodinia supercontinents. In this study, we present detailed U-Pb ages and Hf-isotope compositions of detrital zircons from sixteen Precambrian samples collected from the KTM, combined with available geochronological and geochemical data, to unravel the Precambrian crustal components of the KTM, provenance of the metasedimentary rocks, affinity of the KTM with other continents, and its paleo-positions in the Columbia and Rodinia supercontinents.

2. Geological background and sample descriptions

Vietnam, located in the eastern Indochina Block, is composed of five tectonic units, the Bac Bo, the Tay Bac, the Truong Son Belt, the Kontum Massif (KTM), and the Nambo Block (Fig. 1a). The KTM in central Vietnam is the largest exposure of Precambrian basement in the Indochina Block (Lan et al., 2003). The massif is bounded by the Truong Son Belt to the north and the Nambo Block to the south, and consists of different-grade metamorphic rocks and Phanerozoic igneous rocks. The east-west striking Tam Ky-Phuoc Son Zone in the north of the KTM represents an ancient suture zone between the KTM and the Truong Son Belt (Faure et al., 2018; Nguyen et al., 2019; Tran et al., 2020) or a paleo-rift belt (Tran et al., 2020). The north-south striking Po Ko Fault in the western KTM subdivides this massif into the western and eastern parts (Lepvrier et al., 2008). Recent geochronological studies reveal Permo-Triassic and early Paleozoic metamorphism in the KTM (Bui et al., 2020; Nakano et al., 2021). Based on metamorphic grades and rock associations, the KTM is subdivided into four lithological units (Fig. 1b): the Kan Nack, Kham Duc, Ngoc Linh, and Dien Binh Complexes.

The Kan Nack Complex is located in the central to southeastern part of the KTM and experienced granulite- to amphibolite-facies metamorphism (Fig. 1b). Two distinct units have been identified based on the petrologic features. The lower unit is composed of two-pyroxene

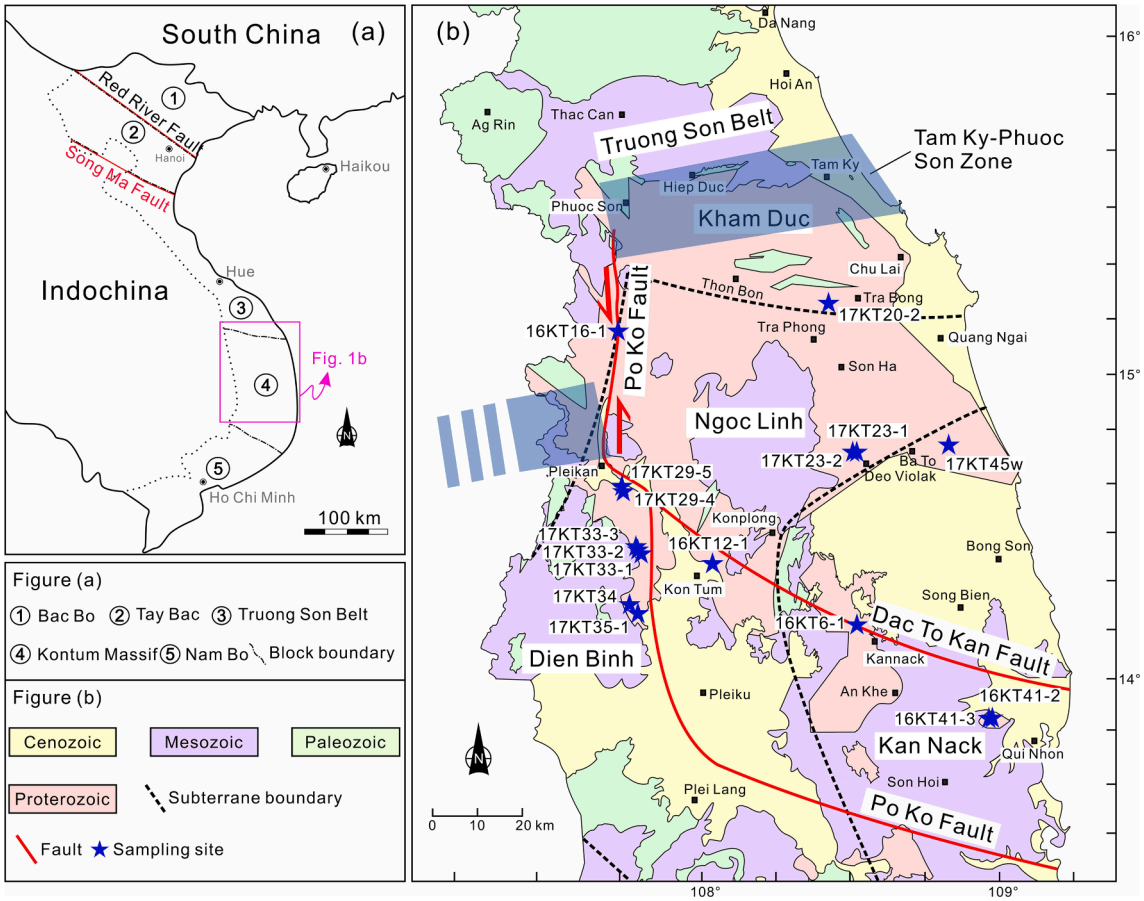

Fig. 1. (a) Simplified tectonic frame map showing different tectonic domains of Vietnam (modified after Jiang et al. (2020)). (b) Sketch geological map of the Kontum Massif and the sample locations (modified after Mineral resources map of Vietnam at 1:1,000,000 scale).

granulites, hypersthene-garnet granulites, and cordierite-sillimanite gneisses, and the upper unit is chiefly represented by garnet-cordierite-sillimanite-biotite gneisses, cordierite-sillimanite schists, and quartzites. In addition, locally mylonitic and dome structures were preserved in the complex, and resulted from intrusive charnockites in the core (Maluski et al., 2005). Samples collected from this lithological unit are granulite (16KT6-1), gneisses (17KT41-2, 17KT41-3) and schist (17KT45w) (Table 1). The granulite 16KT6-1, showing intercalated contact with other rocks, is dark gray (Fig. 2a), and composed of ~45% plagioclase, ~15% hypersthene, ~15% garnet, ~15% quartz, ~5% biotite, and minor magnetite and ilmenite. Samples 17KT41-2 and 17KT41-3 were collected from the eastern part of the Kan Nack Complex and have similar mineral assemblages of garnet (~5%), sillimanite (~5%), biotite (~17%), plagioclase (~35%), K-feldspar (~20%), and quartz (~20%) (Fig. 2b). Garnet porphyroblasts are often altered and show the metasomatic pseudomorph textures. A schist sample 17KT45w consists of ~50% quartz, ~15% feldspar, ~25% mica, and ~5% garnet (Fig. 2c).

The Kham Duc Complex is in the northern KTM (Fig. 1b) and has a general metamorphic grade of upper-greenschist to amphibolite facies. It comprises meta-volcanic rocks in the lower unit, marble and metapelite in the middle unit, and metapelite and metagreywacke in the upper unit. Ultramafic-mafic rocks outcrop as scattered blocks in the metasedimentary suite in the northern part of this area (Faure et al., 2018). They were defined as the Hiep Duc complex and interpreted as a dismembered ophiolitic series (Nguyen et al., 2019). The whole Kham Duc Complex has been described as an accretionary mélange (Nguyen et al., 2019; Faure et al., 2018). Sample 17KT20-2 from this domain is a biotite gneiss and comprises ~30% quartz, ~30% plagioclase, ~10 % K-feldspar, and ~25% biotite (Fig. 2d).

The Ngoc Linh Complex is in the center of the KTM (Fig. 1b) and composed mainly of amphibolite-facies metamorphic rocks. High-grade metamorphic rocks are present in the western section, while relatively low-grade granitic gneisses are widely distributed in the eastern part (Nakano et al., 2013). The Ngoc Linh Complex is subdivided into the Tac Po Formation to the southwest and the Song Re Formation to the northeast. The Tac Po Formation, including two-pyroxene granulites and garnet-orthopyroxene-biotite gneisses, was strongly deformed and mylonitized along the NW-SE trending DTK belt (Osanai et al., 2004). The Song Re Formation consists predominantly of amphibolite-facies metamorphic rocks, such as amphibolites, hornblende-biotite gneisses, biotite-sillimanite gneisses, and garnet-biotite gneisses (Osanai et al., 2004). Collected samples include schists (16KT12-1 and 16KT16-1), leptynite (17KT23-1) and gneiss (17KT23-2) (Table 1). A schist 16KT12-1, intercalated with grayish-yellow gneiss (Fig. 2e), includes ~50% quartz, ~20% plagioclase, ~15% biotite, and minor accessory minerals such as sillimanite, apatite, and epidote. Schist 16KT16-1 is light gray and associated with amphibolite (Fig. 2f). It is composed of ~40% mica, ~20% feldspar, and ~35% quartz. A leptynite sample 17KT23-1 is massive (Fig. 2g) and characterized by elongated and oriented quartz (~60%) and less amphibole and epidote. Sample 17KT23-2 contains ~35% elongated quartz, ~30% plagioclase, ~20% hornblende, and ~7% orientated biotite.

The Dien Binh Complex is situated in the western KTM and separated from the Ngoc Linh Complex by the Po Ko Fault (Fig. 1b). The western boundary of this complex is unclear. It consists of amphibolite- to greenschist-facies metamorphic rocks and Phanerozoic granodioritic to dioritic bodies, aplitic veins, and mafic dykes (Lepvrier et al., 2008). These plutons intrude these metasedimentary rocks consisting of paragneiss, sillimanite-bearing mica schist, and quartzite. Samples collected from this area are gneisses (17KT29-4, 17KT29-5 and 17KT34), and quartz schists (17KT33-1, 17KT33-2 and 17KT33-3) (Table 1). Gneisses 17KT29-4 and 17KT29-5 are dark grayish, moderate grained and gneissose. They have similar mineral components, but sample 17KT29-4 contains relatively more biotite and sillimanite. Sample 17KT34, exposed near the Thac Yali water reservoir (Fig. 2h), consists of ~20% quartz, ~50% plagioclase, ~15 % K-feldspar, and ~15% biotite; half of the feldspar grains are altered to sericite and biotite is partially altered to chlorite. Samples 17KT33-1 and 17KT33-2 are fine-grained schists and have similar mineral components (Fig. 2i), comprising 40–50% quartz and 50–45% muscovite with minor Fe-Ti oxides, whereas sample 17KT33-3 has fine-grained quartz up to ~85% with less muscovite and tourmaline.

3. Analytical techniques

3.1. Zircon U-Pb dating

Zircon grains were separated using conventional magnetic and heavy-liquid separation techniques. Zircon grains were handpicked under a binocular microscope from the concentrated heavy minerals, mounted in epoxy disks and polished to expose their cores. Cathodoluminescence (CL) imaging was carried out to define the morphology and internal structure of zircons and to choose potential target sites for U-Pb dating and Hf-isotope analyses. Zircon U-Pb isotope analyses were performed at the State Key Laboratory for Mineral Deposits Research, Nanjing University, China, with three samples (16KT6-1, 16KT12-1 and 16KT16-1) using an Agilent 7500a ICP-MS equipped with a New Wave 213 nm laser ablation system, and other thirteen samples using iCAP RQ ICP–MS attached to a GeoLas 193 nm laser

Table 1
Lithology and locations of meta-sedimentary rocks from the Kontum Massif, central Vietnam.

Sample No.	Lithology	Location	Longitude	Latitude	Deposition time	Max age (Ma)	Min age (Ma)	Group
17KT23-1	ep-chl schist	NLC	108°33′42.12″	14°44′21.12″	Late Neoproterozoic - Early Paleozoic	<613	>510	G5
17KT23-2	bt-amp schist	NLC	108°33′42.12″	14°44′21.12″		<607		
17KT20-2	bt gneiss	KDC	108°24′32.76″	15°12′21.96″		<1086		
17KT33-1	qtz schist	DBC	107°51′24.44″	14°24′53.64″	Late Mesoproterozoic - Late Neoproterozoic	<1039	>810	G4
17KT29-5	bt gneiss	DBC	107°48′55.44″	14°38′49.92″		<1072		
17KT29-4	sil-bt gneiss	DBC	107°48′55.44″	14°38′49.92″		<1101		
17KT33-2	qtz schist	DBC	107°51′24.44″	14°24′53.64″	Mesoproterozoic	<1360	>1100	G3
17KT41-2	sil-grt gneiss	KNC	108°59′31.66″	13°50′38.00″		<1411		
17KT41-3	grt-bt gneiss	KNC	108°59′31.66″	13°50′38.00″		<1442		
17KT33-3	qtz schist	DBC	107°51′24.44″	14°24′53.64″		<1544		
17KT45w	mica schist	KNC	108°52′51.62″	14°44′54.79″	Late Paleoproterozoic - Early Mesoproterozoic	<1621	>1450	G2
17KT34	gneiss	DBC	107°47′50.32″	14°13′15.49″		<1741		
17KT35-1	gneiss	DBC	107°48′56.26″	14°12′43.85″	Late Paleoproterozoic	<1803	>1650	G1
16KT6-1	granulite	KNC	108°34′32.08″	14°10′12.84″		<1846		
16KT12-1	sil-schist	NLC	108°05′01.99″	14°22′10.51″		<1856		
16KT16-1	schist	NLC	107°45′09.97″	15°08′32.32″		<1815		

Note: KDC – Kham Duc Complex; NLC – Ngoc Linh Complex; KNC – Kannack Complex; DBC – Dien Binh Complex. qtz – quartz, ep – epidote, bt – biotite, sil – sillimanite, grt – garnet.

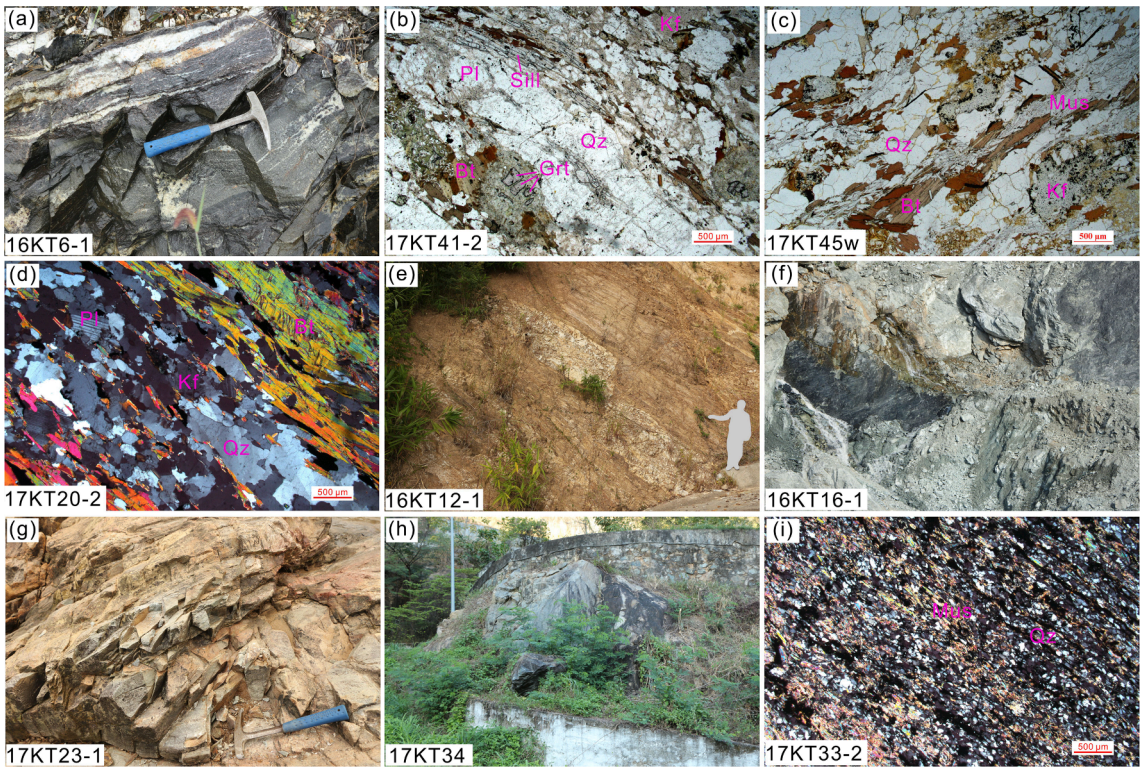

Fig. 2. Field and microscope photographs of the representative samples collected from the Kontum Massif. Grt–garnet; Pl–plagioclase; Qz–quartz; Sill–sillimanite; Mus–muscovite; Kf–K-feldspar.

ablation system. The laser beams were set at 32 μm in diameter, a repetition rate of 5 Hz, and an energy of 10–20 J cm^{-2}. Zircon standard GJ-1 ($^{207}Pb/^{206}Pb$ age of 600 ± 15 Ma) was used to correct the U-Pb isotopic fractionation. Another zircon standard Mud Tank (age of 732 ± 5 Ma) was used to monitor the accuracy and stability of the instrument. Detailed analytical procedures are similar to those described by Griffin et al. (2004). The raw signal data were processed using the software GLITTER (version 4.4) (https://www.mq.edu.au/GEMOC; Griffin et al., 2008). An EXCEL program ComPbCorr#3 15G is used to carry out common Pb correction for younger ($^{206}Pb/^{238}U$ < 540 Ma) grains according to the method proposed by Andersen (2002). ISOPLOT (version 4.15, Ludwig, 2003) was used to calculate ages and plot Concordia diagrams. In general, $^{207}Pb/^{206}Pb$ ages are accepted for zircons with $^{207}Pb/^{206}Pb$ age > 900 Ma (Yu et al., 2010) and $^{206}Pb/^{238}U$ ages for those younger grains. The zircon U-Pb dating results are presented in Table S1.

3.2. Hf isotopes in zircons

In situ Lu-Hf isotopic analyses of zircons were conducted using a Neptune Plus multi-collector ICP-MS attached with a GeoLas 193 nm ArF3 laser ablation system at the State Key Laboratory for Mineral Deposits Research in Nanjing University. Hf-isotope analysis spots are in the same or similar zircon domains to those for U-Pb dating. Laser ablation pits are 44 μm in diameter and laser repetition rate is 10 Hz. The standard zircon 91500, whose $^{176}Hf/^{177}Hf$ value is 0.282300 ± 8 (2σ), was analyzed before the unknowns to check the reliability and stability of the instrument. Detailed analytical procedures are similar to those described by Yuan et al. (2003). The measured $^{176}Hf/^{177}Hf$ ratios and a ^{176}Lu decay constant of 1.865×10^{-11} $year^{-1}$ (Scherer et al., 2001) were used to calculate initial $^{176}Hf/^{177}Hf$ ratios, and a chondritic model with $^{176}Hf/^{177}Hf = 0.282772$ and $^{176}Lu/^{177}Hf = 0.0332$ (Blichert-Toft and Albarede, 1997) was adopted in the calculation of εHf values. To calculate the depleted mantle Hf model ages (T_{DM}) and two-stage crustal model ages (T_{DM}^{C}), the depleted mantle with $^{176}Hf/^{177}Hf = 0.283250$ and $^{176}Lu/^{177}Hf = 0.0384$ and the $^{176}Lu/^{177}Hf$ of average continental crust (0.015; Griffin et al., 2002) were used. The zircon Lu-Hf isotope results are presented in Table S2.

4. U-Pb ages and Hf isotopes of zircon grains

4.1. Zircon U-Pb ages

Zircon grains from sixteen metasedimentary rocks show euhedral to elliptical shapes with variable sizes (Fig. 3). CL images show that most grains have inherited cores with oscillatory compositional zoning and narrow overgrowth rims. Most cores have Th/U ratios of > 0.4 (Table S1), suggesting their magmatic origins. About ten percentage of grains exhibit sector, soccer-shape, or homogeneous internal textures with low Th/U (<0.1), interpreted as metamorphic zircons.

Detrital zircons from sample 16KT6-1 have concordant (concordance of 95–105%) ages ranging from 2527 Ma to 1654 Ma, and those from sample 16KT12-1 straddle from 3212 Ma to 1714 Ma (Table S1). Both samples have two major groups of detrital zircons, Neoarchean-early Paleoproterozoic and late Paleoproterozoic ones. They define two discordia lines and yield upper intercepts of 2560–2498 Ma and 1846–1856 Ma (Fig. 3a-b), respectively, approximating two remarkable age peaks (Fig. 4a-b). Sample 17KT35-1 has a similar detrital age distribution (2996–1712 Ma) to the above two samples (Fig. 3c). Late Paleoproterozoic zircon grains define a discordia with an upper intercept of 1803 Ma, similar to the major peak at 1802 Ma (Fig. 3c, 4c).

Sample 16KT16-1 mainly contains late Paleoproterozoic zircons. The discordant grains define a discordia with an upper intercept of 1815 Ma and a lower intercept of 450 Ma (Fig. 3d). Four older grains give discordant ages of 2624 to 2420 Ma. This sample contains two groups of metamorphic zircons with ages of 507–418 Ma and 275–253 Ma, respectively (Table S1).

Samples 17KT34 and 17KT45w also include two main age

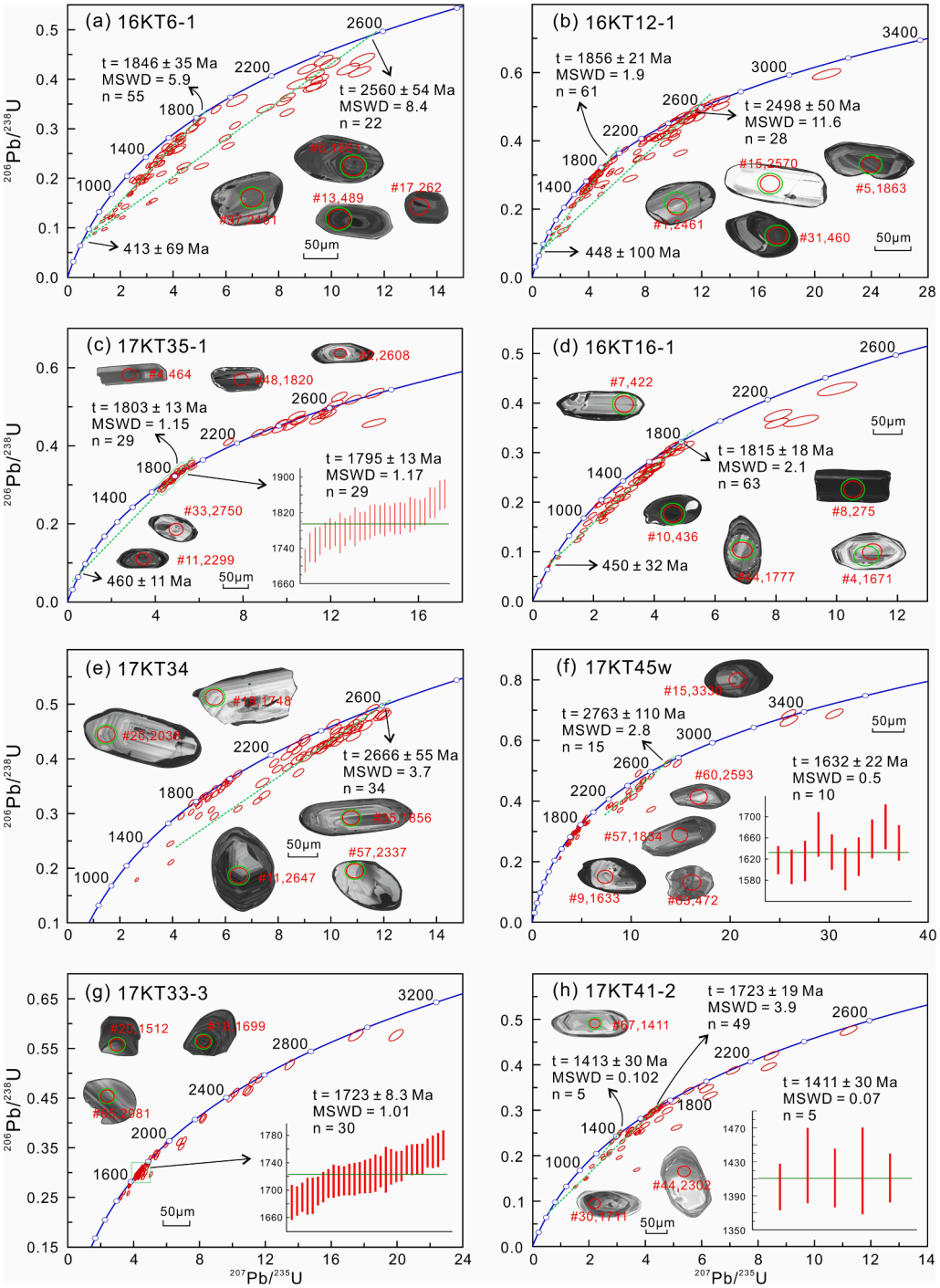

Fig. 3. U-Pb Concordia diagrams of zircons from meta-sedimentary rocks in the Kontum Massif. Ages shown at the intercept of the Discordia are the upper and lower intercept ages.

populations, Neoarchean and late Paleoproterozoic (Fig. 3e-f; Table S1). Neoarchean zircon populations yield upper intercept ages of 2666 Ma and 2763 Ma, respectively, whereas late Paleoproterozoic populations have adundant concordant grains younger than 1800 Ma, with peaks at 1747 Ma and 1636 Ma (Fig. 4e-f). In addition, sample 17KT34 contains some early Paleoproterozoic (~2366 Ma) grains (Fig. 3e).

Sample 17KT33-3 has many concordant or near-concordant (concordance = 95–90%) detrital zircons with ages ranging from 3190 Ma to 1512 Ma (Fig. 3g). These ages define a main peak of 1727 Ma and three subordinate peaks at 2570 Ma, 2295 Ma, and 1534 Ma (Fig. 4g). Thirty concordant late- Paleoproterozoic zircons yield a weighted mean age of 1723 ± 8.3 Ma. Three youngest detrital zircons have concordant ages of 1589 to 1512 Ma.

Samples 17KT41-2, 17KT41-3, and 17KT33-2 have abundant late Paleoproterozoic and Mesoproterozoic detrital zircons. Most zircons are concordant or near-concordant, and form two significant age peaks at 1710–1729 Ma and 1447–1416 Ma (Fig. 4h-j). These two zircon groups define two discordia lines. The upper intercepts of discordia lines constrained by late Paleoproterozoic zircons of three samples are 1723 ± 19 Ma, 1725 ± 17 Ma, and 1755 ± 17 Ma, and the upper intercept ages

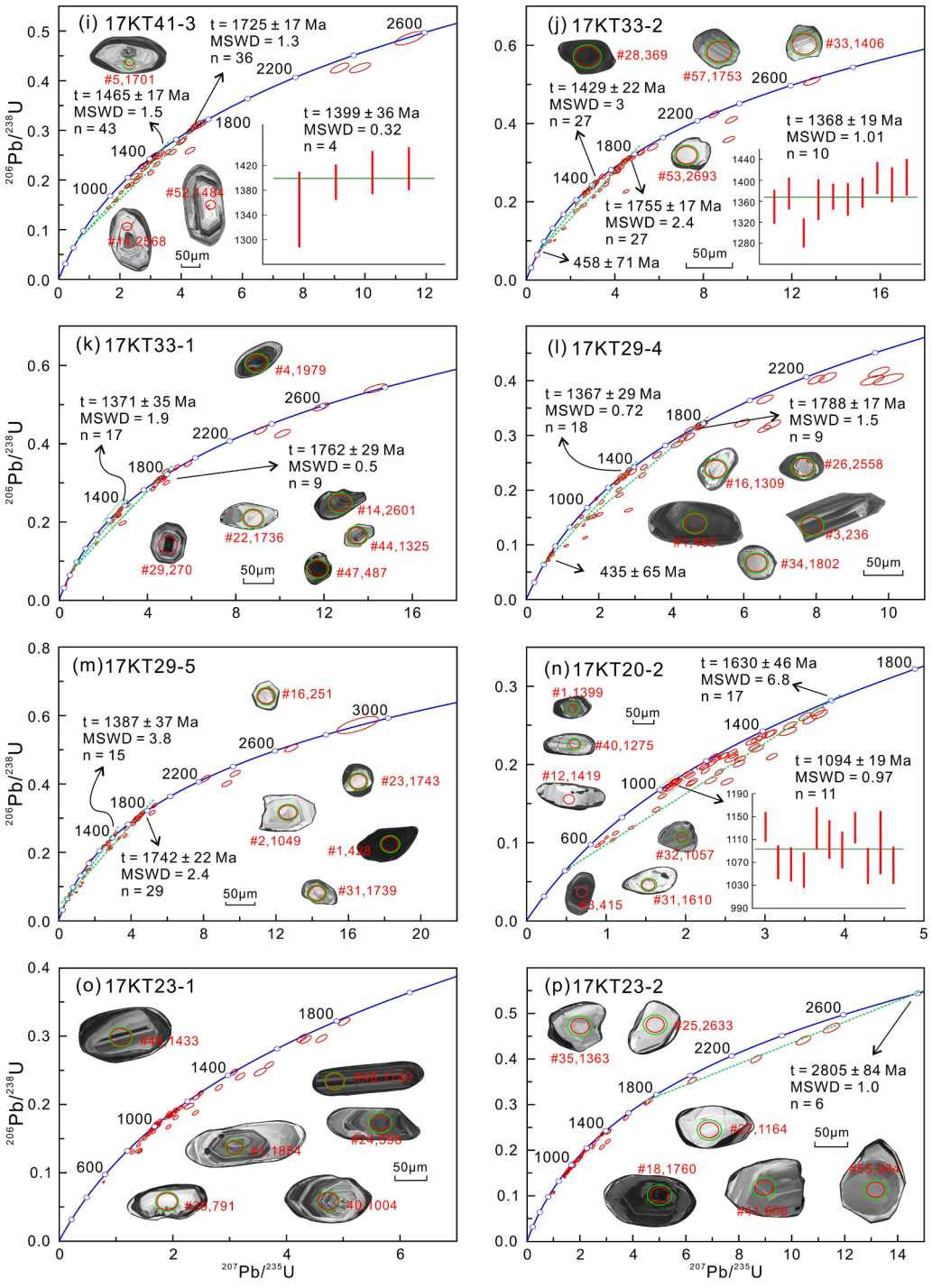

Fig. 3. (*continued*).

constrained by Mesoproterozoic zircons are 1413 ± 30 Ma, 1465 ± 17 Ma, and 1429 ± 22 Ma (Fig. 3h-j). These samples all contain minor Neoarchean (2568–2693 Ma) and Paleoproterozoic (2355–1989 Ma) grains. The youngest detrital zircons in the three samples have concordant ages of 1401 Ma, 1349 Ma and 1300 Ma respectively.

Samples 17KT33-1, 17KT29-4 and 17KT29-5 have detrital-zircon age distribution similar to the above three samples (Fig. 3k-m, 4k-m). However, they have more Ectasian (1400–1200 Ma) and fewer Archean to early Paleoproterozoic zircons. The discordant detrital zircons of sample 17KT33-1 yield two upper intercepts of 1762 ± 29 Ma and 1371 ± 35 Ma (Fig. 3k). Those of sample 17KT29-4 define two discordia lines with upper intercepts of 1788 ± 17 Ma and 1367 ± 29 Ma (Fig. 3l), and those of 17KT29-5 form two discordia lines with upper intercepts of 1742 ± 22 Ma and 1387 ± 37 Ma (Fig. 3m). These upper intercept ages are consistent with the two major age peaks (Fig. 4k-m). The youngest detrital-zircon ages in these three samples are 1039 Ma, 1101 Ma, and 1049 Ma, younger than the aforementioned samples.

Sample 17KT20-2 is characterized by abundant Mesoproterozoic detrital zircons with a continuous age range straddling from 1646 Ma to 1057 Ma (Fig. 3n, 4n). Eleven young concordant detrital zircons yield a weighted mean of 1094 ± 19 Ma (Fig. 3n). Samples 17KT23-1 and 17KT23-2 show similar detrital-zircon age populations, characterized by abundant Mesoproterozoic and less late Paleoproterozoic ages with a main peak at *ca* 1050–1000 Ma (Fig. 4o-p; Table S1), similar to sample

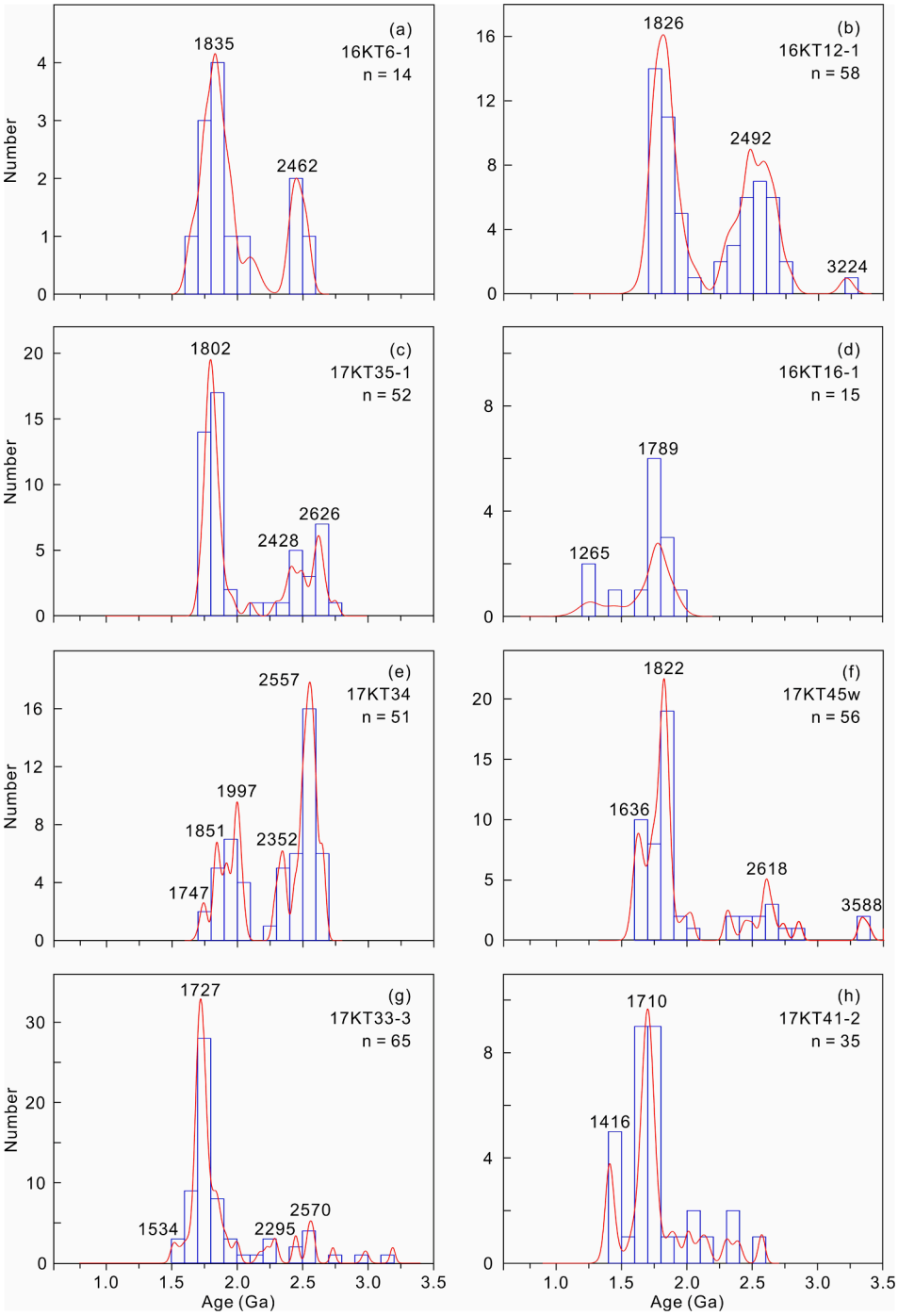

Fig. 4. Relative probability density diagrams and histograms of ages with concordance > 90%.

17KT20-2. However, these two samples have adundant younger (<1000 Ma) grains (Fig. 3o-p), even down to 651–606 Ma.

4.2. Zircon Hf-isotope compositions

Zircons from fourteen samples show variable Hf-isotope compositions (Fig. 5). Samples 16KT6-1 and 16KT12-1 from the Kan Nack and Ngoc Lihn complexes have not only similar detrital zircon ages but also similar Hf-isotope compositions. Their late Neoarchean to early Paleoproterozoic detrital zircons have juvenile Hf-isotope compositions, whereas the late Paleoproterozoic zircons show large Hf-isotope variations with εHf(t) values of +13.9 to −12.1 (Fig. 5a; Table S2). Late Paleoproterozoic zircons and a few ~2.5 Ga grains of sample 16KT16-1 have Hf-isotope compositions overlapping with those in samples 16KT6-1 and 16KT12-1 (Fig. 5a).

Although sample 17KT34 from the Dien Binh Complex has detrital zircon components similar to those of samples 16KT6-1 and 16KT12-1, its Neoarchean and late Paleoproterozoic zircons have much low εHf(t) values (Fig. 5a), distinct from those of samples 16KT6-1 and 16KT12-1. However, sample 17KT33-3 in the Dien Binh Complex shows zircon Hf-isotope compositions similar to samples 16KT6-1 and 16KT12-1 (Fig. 5a-b).

Samples 17KT41-2, 17KT41-3, 17KT33-1, 17KT33-2, 17KT29-4, and 17KT29-5 all contain 1.80–1.70 Ga and 1.45–1.35 Ga detrital zircons,

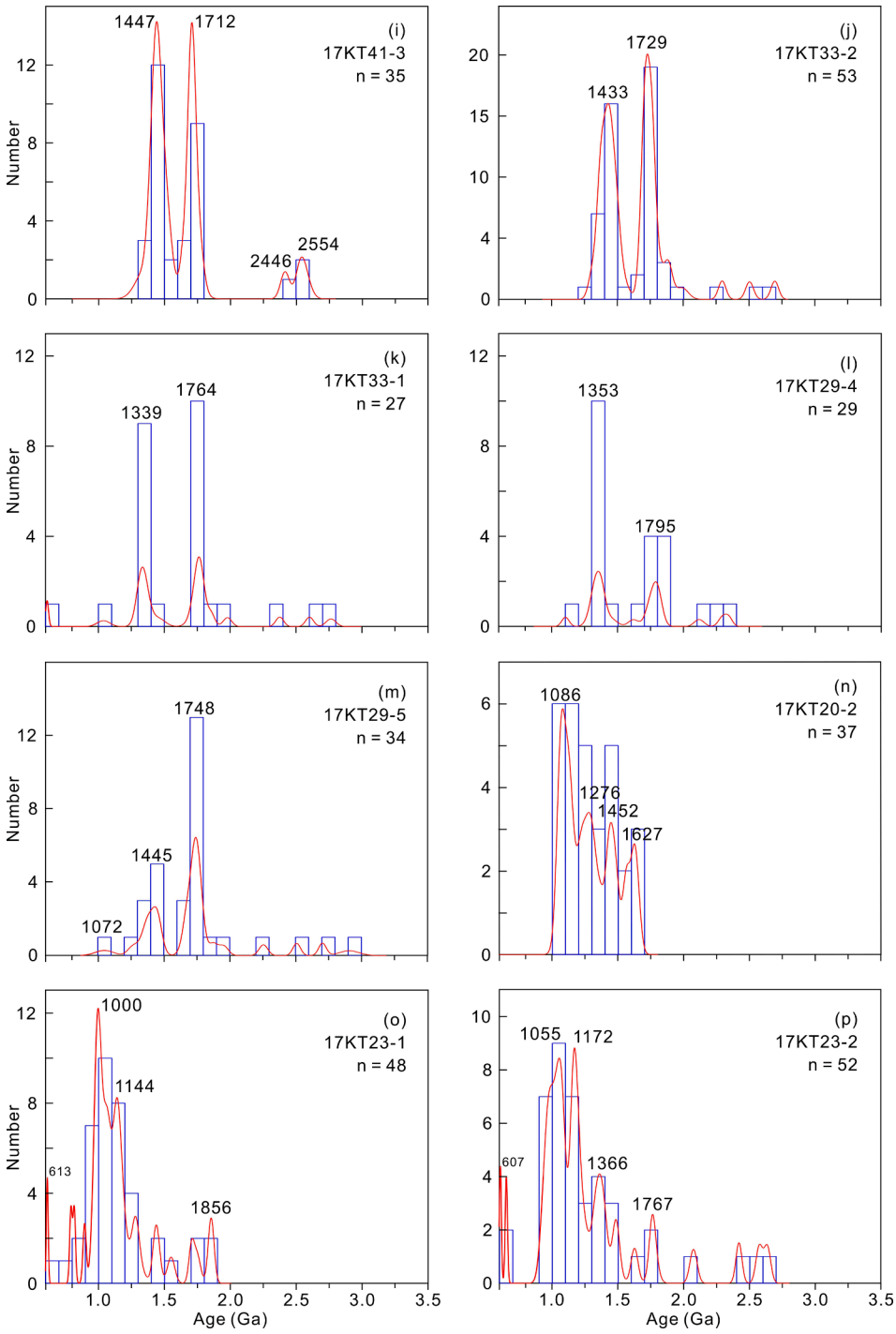

Fig. 4. (*continued*).

but their zircon Hf-isotope compositions are different (Fig. 5b-c). The ~1.7 Ga and ~1.4 Ga detrital zircons in samples 17KT41-2 and 17KT41-3 from the eastern Kan Nack Complex have negative εHf(t) values except for two grains, whereas the Mesoproterozoic zircons of the other four samples from the Dien Binh Complex predominantly exhibit positive εHf (t) (Fig. 5b). The 1.8–1.7 Ga zircons are also characterized by dominant positive εHf(t) except those in sample 17KT33-1 (Fig. 5c), implying that the clastic debris in sedimentary rocks in two complexes came from different sources.

Although samples 17KT20-2, 17KT23-1, and 17KT23-2 have similar detrital zircon age spectra, almost all of detrital zircons in sample 17KT20-2 from the Kham Duc Complex have positive εHf(t), different from those in samples 17KT23-1 and 17KT23-2 from the Ngoc Linh Complex (Fig. 5d), also suggesting that they were derived from different provenances.

5. Discussion

5.1. Formation and metamorphic ages of the KTM basement rocks

The KTM was regarded as an Archean (>2.6 Ga) terrane based on the high-grade metamorphic rock association (Hutchison, 1989). However, Archean rocks with accurate isotopic ages have not been identified in this massif. Nakano et al. (2021) proposed that the 1470–1432 Ma mafic

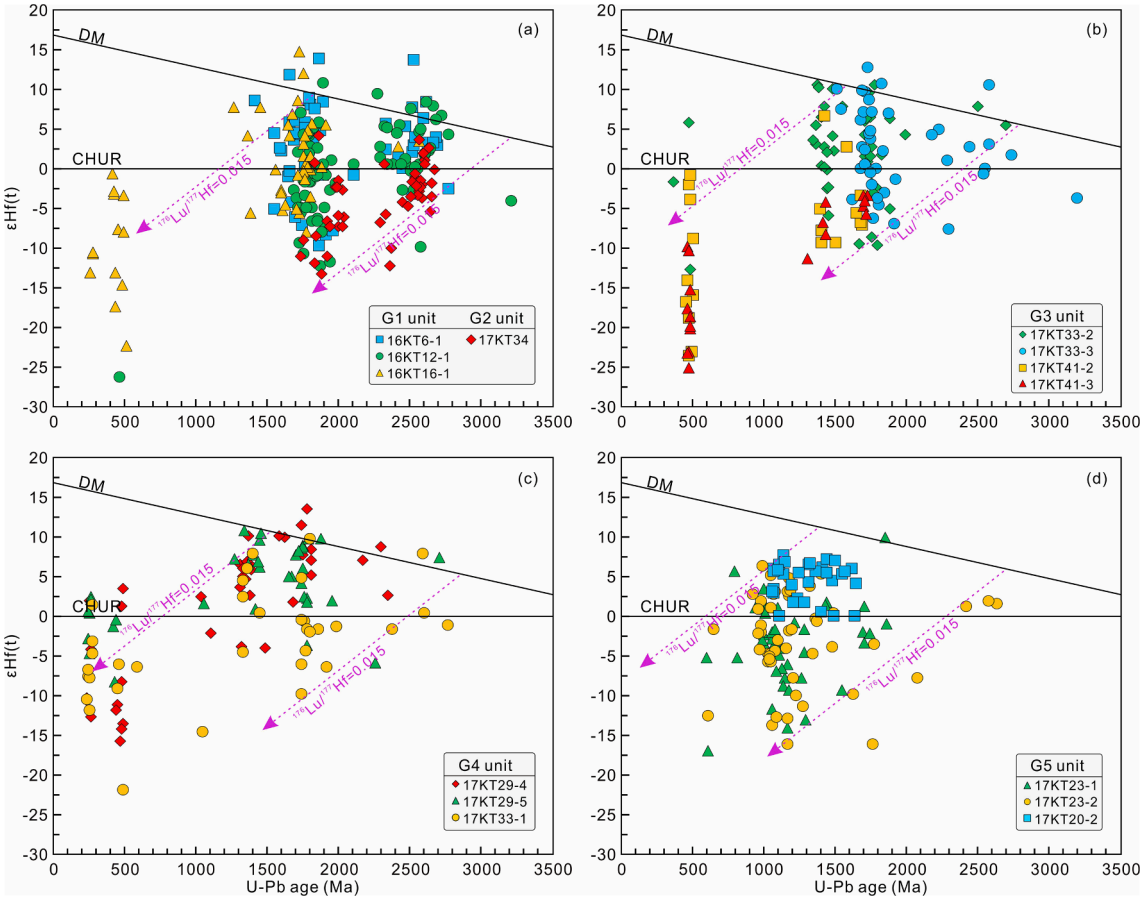

Fig. 5. Hf isotope compositions of detrital zircons from the representative samples.

and felsic magmatism represents the early or primary stage of the formation of the KTM. However, new data in this study show that the KTM basement probably formed earlier than the Mesoproterozoic Era.

Metasedimentary rocks in the KTM have complicated detrital-zircon components, indicating different depositional ages and provenances. Samples 16KT6-1, 16KT12-1, 17KT35-1, and 16KT16-1 have predominant late Paleoproterozoic detrital zircons without younger ones (Fig. 4a-d). Their discordant Paleoproterozoic detrital zircons define discordia lines, yielding upper intercepts of 1856 to 1803 Ma (Table 1; Fig. 3a-d). These upper intercept ages may represent their depositional ages, and can be used to constrain the maximum depositional ages of these sedimentary rocks. They all lack 1.72–1.63 Ga detrital zircons (Fig. 4a-d), which are abundant in sample 17KT45w and the younger sedimentary rocks. Thus, these four meta-sedimentary rocks were probably deposited at 1.85–1.63 Ga, before intrusion of the ~1.45 Ga magmatic rocks.

Sample 17KT34 has fewer late Paleoproterozoic detrital zircons with scattered ages (Fig. 3e). The two youngest detrital zircons give concordant ages of 1748 Ma and 1733 Ma, with a mean age of 1741 Ma. Sample 17KT45w contains abundant and variable late Paleoproterozoic detrital zircons. Ten concordant youngest detrital zircons have ages of 1681–1601 Ma, yielding a mean age of 1632 ± 22 Ma (MSWD = 0.50) (Fig. 3f). These two samples lack the 1.54–1.40 Ga detrital zircons (Fig. 4e-f) that are abundant in the younger sedimentary rocks, consequently constraining their deposition in the late Paleoproterozoic to early Mesoproterozoic.

The three youngest detrital zircons in sample 17KT33-3 have concordant ages of 1589–1512 Ma (Table S1), giving a mean age of 1544 Ma. Samples 17KT33-2, 17KT41-2, and 17KT41-3 have abundant Mesoproterozoic and late Paleoproterozoic detrital zircons (Fig. 4h-j). The youngest concordant detrital zircons in these three samples yield weighted mean ages of 1368 ± 19 Ma, 1411 ± 30 Ma, and 1399 ± 37 Ma (Fig. 3h-j), respectively, suggesting that these sedimentary rocks were deposited later than 1368–1411 Ma. These samples do not contain 1100–1000 Ma detrital zircons which are abundant in many younger sedimentary rocks, such as samples 17KT20-2, 17KT23-1, and 17KT23-2 (Fig. 4k-p). Therefore, these four sedimentary rocks were most likely to be deposited in the late Mesoproterozoic, about 1.5–1.1 Ga.

Samples 17KT33-1, 17KT29-4, and 17KT29-5 also have two main age populations at late Paleoproterozoic (1.79–1.75 Ga) and Mesoproterozoic (1.44–1.34 Ga), but their younger (~1.35 Ga) detrital zircons markedly increase relative to above-mentioned samples (Fig. 4k-m). On the other hand, they all contain a few late Mesoproterozoic (Grenvillian) detrital zircons with ages of 1101–1039 Ma, constraining their deposition after 1101–1039 Ma. These three samples lack the middle to late Neoproterozoic (816–606 Ma) detrital zircons, suggesting their deposition occurred in the Neoproterozoic (>*ca* 810 Ma).

Samples 17KT23-1 and 17KT23-2 contain abundant Grenvillian detrital zircons (Fig. 4o-p). The youngest grains have ages of 598–651 Ma, with a mean age of 610 Ma, suggesting that their deposition was not earlier than *ca* 610 Ma. Sample 17KT20-2 in the northern KTM also has abundant Mesoproterozoic detrital zircons (Fig. 4n), similar to samples 17KT23-1 and 17KT23-2, implying their similar provenances and deposition ages, even though it does not contain Neoproterozoic zircons. Extensive early Paleozoic (476–440 Ma) magmatism and metamorphism occurred in the KTM (Nguyen et al., 2019; Jiang et al., 2020; Tran et al., 2020; this study). 518–502 Ma plagiogranites have been identified in the northern KTM, near sample 17KT20-2 (Nguyen et al., 2019). Hence, the absence of early Paleozoic detrital zircons suggests that these sedimentary rocks were probably deposited in the late Neoproterozoic to early Paleozoic (*ca* 518–610 Ma; Table 1).

Almost all samples suffered late tectonothermal events. Our

geochronological data suggest that the KTM mainly experienced two periods of metamorphism, in the early Paleozoic (501–415 Ma) and Indosinian (275–235 Ma). Early Paleozoic zircons generally have low Th/U (most < 0.1) and internal structures typical of metamorphic zircons, suggesting their subsolidus metamorphic origin. This thermal event affected almost the whole KTM with high-grade metamorphism up to granulite-facies locally. In contrast, most Indosinian zircons have high Th/U (>0.4), and some show oscillatory compositional zoning, similar to magmatic zircons. This thermal event mainly influenced the western part of the KTM. In addition, some samples from the Dien Binh Complex, including Mesoproterozoic gneissic granite (Wang et al., 2020), record a late Paleozoic (371–331 Ma) tectonothermal imprint (Table S1).

5.2. Components of basement rocks and their origin

New results indicate that the Precambrian basement of the KTM consists of a great variety of sedimentary rocks with different formation ages and lesser Mesoproterozoic igneous rocks. The sedimentary rocks were subdivided into five units (Table 1). The first unit of sedimentary rocks (G1) formed in the late Paleoproterozoic (*ca* 1.85–1.65 Ga), and presents the oldest rocks found in the KTM to date. The second unit of sedimentary rocks (G2) was deposited in the late Paleoproterozoic to early Mesoproterozoic (*ca* 1.74–1.45 Ga), and the third unit (G3) in the Mesoproterozoic (*ca* 1.5–1.1 Ga) is accompanied by coeval mafic and felsic magmatism (Wang et al., 2020; Nakano et al., 2021). The fourth unit of sedimentary rocks (G4) was generated in the latest Mesoproterozoic to middle Neoproterozoic (*ca* 1.10–0.81 Ga), and the fifth unit (G5) in the late Neoproterozoic to early Paleozoic (0.61–0.51 Ga). No Archean rocks have been identified in this study, despite the abundance Archean detrital zircons in the sedimentary rocks.

Different units of sedimentary rocks in the KTM have distinct detrital zircon components. The G1 sedimentary rocks mainly contain Neoarchean and late Paleoproterozoic detrital zircons with three major peaks at ~1.80 Ga, ~2.63 Ga, and ~2.49 Ga (Fig. 6a). The Neoarchean-early Paleoproterozoic zircons have positive εHf(t) values except for a few grains (Fig. 7a), indicating an important period of juvenile crust growth in the source area. Late Paleoproterozoic zircons show large ranges in εHf(t) (Fig. 7a). Those zircons with the lowest εHf(t) lie on the evolutionary trend of the Neoarchean zircons (Fig. 7a), suggesting that their host magma was derived from these Neoarchean materials. A great number of late Paleoproterozoic zircons have juvenile εHf(t), even up to the DM evolution line (Fig. 7a), suggesting a large-scale mantle-derived magmatic activity along with ancient crust reworking. The combination of these magmatic processes suggests a continental-arc setting, which is consistent with an arc-related sedimentary setting or the active continental margin inferred from the geochemistry of the sedimentary rocks

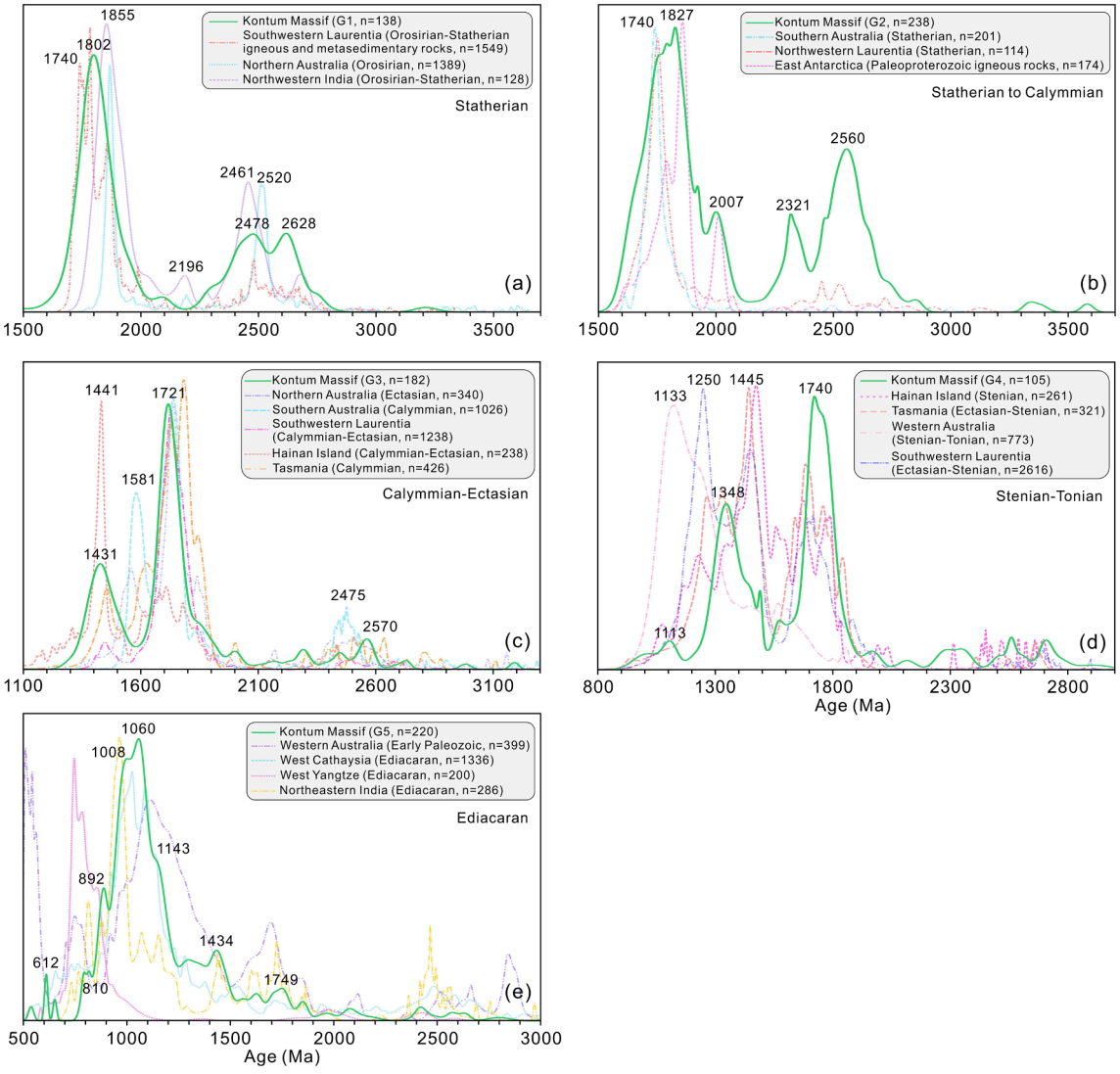

Fig. 6. Age spectra of detrital zircons from five periods of sedimentary rocks in the KTM and the equivalent sedimentary rocks from different cratons or microcontinents. Only data with > 90% concordance are used. Data details are given in Table S3.

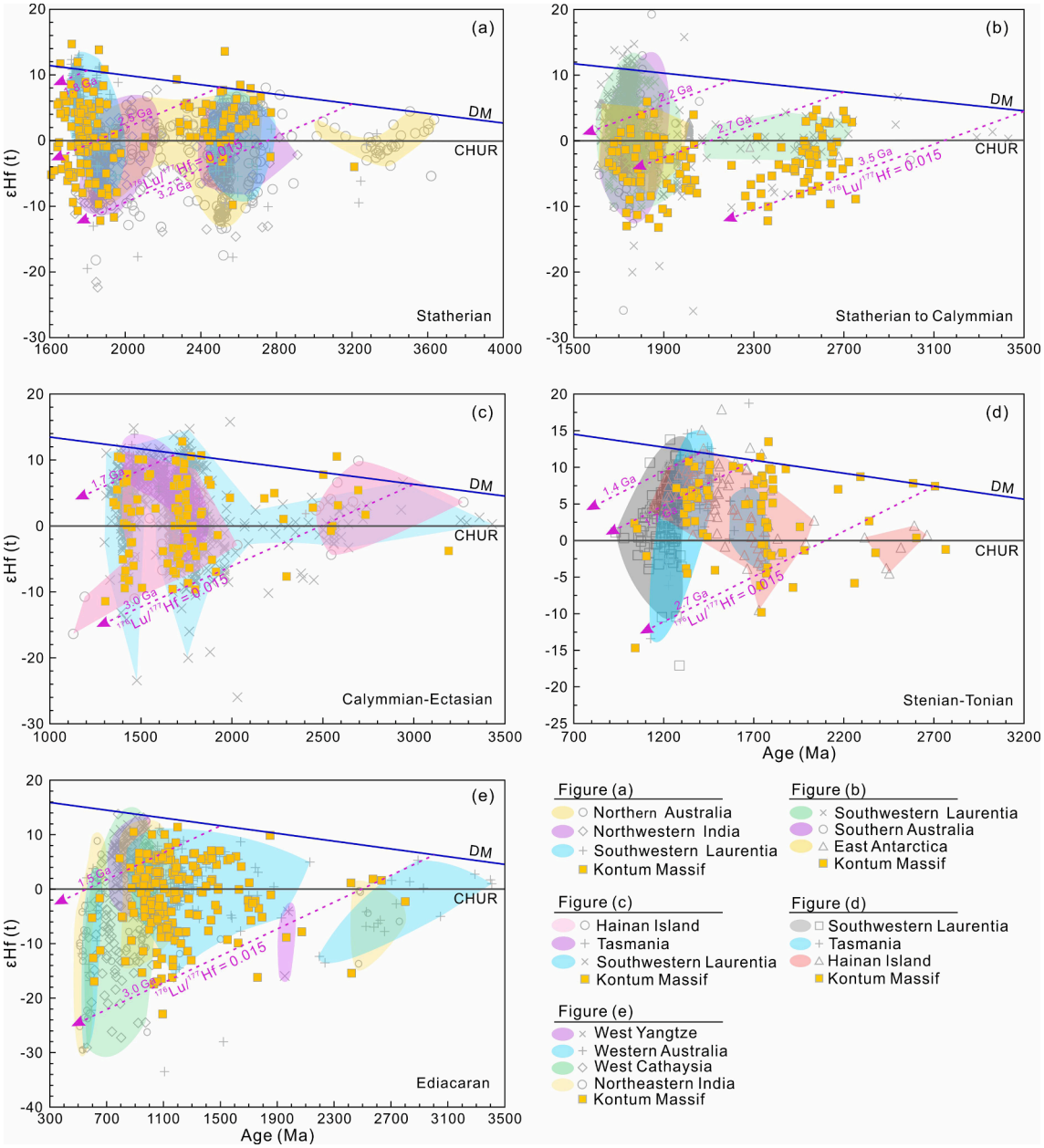

Fig. 7. Diagrams of εHf(t) vs. U-Pb ages for the detrital zircons from the Kontum Massif and other continents and microcontinents. Data details are given in Table S4.

by Wang et al. (2020).

The G2 sedimentary rocks have detrital zircon age spectra similar to the G1, except for a weak peak of ~2.32 Ga and significantly more 1.75–1.65 Ga zircons (Fig. 6b). However, both Neoarchean-early Paleoproterozoic and late Paleoproterozoic zircons are characterized by low εHf(t), different from those of the G1 (Fig. 7b), indicating a decrease in the arc magmatic clastics in the G2. Geochemical features also imply that the G2 sedimentary rocks were deposited in a passive continental margin (Wang et al., 2020).

The G3 sedimentary rocks are characterized by two major zircon age populations of ~1.72 Ga and ~1.44 Ga with a minor ~2.57 Ga population (Fig. 6c). The Neoarchean and late Paleoproterozoic zircons have Hf-isotope compositions similar to those of the G1 (Fig. 7c), suggesting similar provenances. Middle Mesoproterozoic zircons from different samples show distinct Hf-isotope compositions (Fig. 5b). Samples 17KT41-2 and17KT41-3 from the eastern Kan Nack Complex have lower zircon $\underline{\varepsilon}$Hf(t) (-11.4 to −4.16), whereas samples 17KT33-3 and 17KT33-2 from the Dien Binh Complex have higher zircon $\underline{\varepsilon}$Hf(t) (-0.14 to 10.6). They mainly derived from felsic and mafic sources, respectively. Geochemical features of these sedimentary rocks also suggest that their detritus were derived from felsic and mafic sources, respectively (Wang et al., 2020). The ~1.44 Ga bimodal magmatism occurred in the KTM (Wang et al., 2020; Nakano et al., 2021), comparable to that in Hainan Island, South China, which is suggested to occur in a rift-related setting (Zhang et al., 2018; Xu et al., 2020).

The G4 metasedimentary rocks have striking age peaks at 1740 Ma and 1348 Ma (Fig. 6d). The ~1.74 Ga components show a large $\underline{\varepsilon}$Hf(t) range (Fig. 7d), similar to those of the G3 samples. The ~1.35 Ga zircons dominantly have positive $\underline{\varepsilon}$Hf(t) (Fig. 7d), similar to those ~1.4 Ga grains in the G3 samples from the Dien Binh Complex, reflecting the extensive middle Mesoproterozoic mafic magmatism in the western KTM.

The G5 sedimentary rocks contain abundant Mesoproterozoic to Neoproterozoic detrital zircons with a major peak at ~1.06 Ga and four minor peaks at ~1.43 Ga, ~0.89 Ga, ~0.81 Ga, and ~0.61 Ga (Fig. 6e). Compared with the above groups, Archean to Paleoproterozoic zircons

significantly decrease, whereas late Mesoproterozoic to Neoproterozoic grains increase, especially Grenvillian ones. Mesoproterozoic zircons show significantly varying Hf-isotope compositions (Fig. 7e), and those from sample 17KT20-2 in the northern KTM have positive εHf(t) (Fig. 5d), suggesting that their sources comprise more juvenile crustal material.

5.3. Paleo-positions of the KTM from Columbia to Gondwana

Where was the KTM or whole Indochina Block from? Reconstructions of supercontinents in the Earth's history are largely based on paleomagnetic data and comparison of the global-scale collisional orogenies (Zhao et al., 2002). However, reconstructions of the Columbia supercontinent are not definite, because Paleoproterozoic paleomagnetic data are scarce and show a large scatter of poles (Evans and Mitchell, 2011). Thus, comparisons of orogenic events among different orogens and cratonic blocks have become essential to determine the linkages between different continents (Zhao et al., 2002). However, zircon age data alone are not enough to strictly constrain the nature of the orogen and the relationship of separated continental fragments. Zircon Lu-Hf isotopic data and whole-rock geochemistry can provide additional constraints (Yu et al., 2012). The integration of these factors provide a rigorous "barcode" to match the signatures of various continental blocks. The five units of sedimentary rocks in the KTM contain complex information on the orogenic events in the KTM and nearby continents, which can be used to constrain the paleo-positions of the KTM in the supercontinents.

5.3.1. Orosirian - Statherian (1.85–1.65 Ga)

The G1 sedimentary rocks with maximum deposition ages in the Orosirian Period contain abundant 2.65–2.40 Ga and ~1.80 Ga detrital zircons (Fig. 6a). The synchronous magmatism has not been reported in the KTM; hence these clastics should be allochthonous. Paleoproterozoic orogenic belts with Neoarchean basement are globally widespread. However, Paleoproterozoic orogenies in many cratons occurred at 1.95–2.25 Ga or on the older (>2.6 Ga) basement, such as the Yangtze Craton of South China, West Africa, South America, South Africa, western Australia, West Greenland, and Siberia cratons (Wang et al., 2016a; Boher et al., 1992; Grochowski et al., 2021; Zeh et al., 2016; Johnson et al., 2011; Gardiner et al., 2019; Rosing et al., 2001). The tectonothermal events in these areas are inconsistent with the age peaks recorded in the G1 sedimentary rocks, and consequently they are excluded as potential sources. Significant 2.60–2.40 Ga orogenies occurred in Laurentia, West Greenland, India, North China, and the Mawson Continent (East Antarctica and the Gawler Craton of southern Australia), and extensive late Paleoproterozoic (~1.85 Ga) magmatism occurred in East Cathaysia, India, northern Australia, the Mawson Continent, North China, and Laurentia. These cratons or blocks are potential sources of the sediments deposited in the G1.

The Paleoproterozoic orogeny in East Cathaysia occurred at 1.90–1.85 Ga on the basement consisting mainly of metasedimentary rocks with dominant ~2.5 Ga detritus (Yu et al., 2012). Late Paleoproterozoic granitic rocks were sourced from this basement and have negative zircon εHf(t) (Yu et al., 2009, 2012), different from those of the G1 (Fig. 7a). Extensive 1.90–1.80 Ga arc-related magmatism took place in the Aravalli-Delhi orogenic belt (Richards et al., 2005; Sen et al., 2019) and the Khetri area (Kaur et al., 2009, 2017) in northwestern India. However, their zircon Hf isotopic compositions are significantly different from those of the G1. Different age spectra and Hf-isotope compositions of detrital zircons from the coeval sequences in northwestern India (Figs. 6a, 7a) further suggest that the Aravalli-Delhi orogenic belt was not in the source area of the G1. Widespread 1.87–1.80 Ga magmatism developed in the Pine Creek Orogen in northern Australia and Neoarchean inliers (~2.5 Ga) in the nearby Granites-Tanami Orogen (Iaccheri and Bagas, 2020). Notably, the Orosirian sedimentary rocks in these orogens have significant detrital-zircon age peaks of 2523 Ma and 1869 Ma similar to that of the G1 (Fig. 6a). However, these zircons show large Hf-isotope composition discrepancies with those of the G1 (Fig. 7a), implying that the KTM was not adjacent to northern Australia at 1.85–1.65 Ga.

The initial cratonization of the North China Craton resulted from the amalgamation of major microcontinents along several granite-greenstone belts during 2.58–2.45 Ga, and the ~1.85 Ga Trans-North China Orogeny lead to the assembly of the eastern and western blocks (Tang and Santosh, 2018; Zhao et al., 2011; Zhai et al., 2015). However, the ~1.85 Ga collisional event is dominated by high-grade metamorphism with minor granitic magmatism. The ~1.85 Ga metamorphic and granitic rocks have low zircon εHf(t) values (Yang et al., 2021; Tang and Santosh, 2018). These signatures are consistent with detrital zircons from modern river sands in North China (Yang et al., 2009), but significantly different from the G1 (Fig. 7a). Therefore, the KTM was unlikely connected with the North China Craton in the late Paleoproterozoic.

Extensive Neoarchean and Paleoproterozoic magmatism and metamorphism are recorded in Laurentia. However, Neoarchean magmatism in northwestern to northern Laurentia mainly occurred at 2.72–2.65 Ga (Breemen et al., 2007; Davis et al., 2006). In northwestern Laurentia, there is not only late Paleoproterozoic but also strong middle Paleoproterozoic magmatism (Furlanetto et al., 2016; Berman et al., 2013; Partin et al., 2014), and consequently the affinity of northwestern Laurentia with the KTM can be excluded. Strong ~2.5 Ga magmatism occurred in southwestern Laurentia, such as the Wyoming Province (Mueller and Frost, 2006; Mueller et al., 2011) and the adjacent Gawler Craton (Mawson Continent) (Hand et al., 2007; Swain et al., 2005; Howard et al., 2009; Reid et al., 2014).

The Paleoproterozoic crust of southwestern Laurentia generally was formed by accretionary orogenesis (Holland et al., 2015, 2018). The arc magmatism and crustal accretion occurred between 1.91 and 1.83 Ga (Schneider et al., 2007), and the terminal collision along the Trans-Hudson Orogen occurred between 1.83 and 1.80 Ga (Breemen et al., 2007). The Orosirian-Statherian sedimentary (such as Vishnu Basin) and igneous rocks in southwestern Laurentia yield a zircon age spectrum with several peaks at 2483 Ma, 1857 Ma, 1784 Ma, and 1742 Ma (Fig. 6a). The two peaks of 2483 Ma and 1857 Ma match well with those of the G1. The ~2.63 Ga detrital materials are enriched in late Paleoproterozoic successions in southwestern Laurentia, which probably were sourced from the Clearwater complex in the southern part of the Wyoming Craton (Holland et al., 2018; Vervoort et al., 2016). The 1784 Ma and 1742 Ma zircon grains are lacking in the G1 but abundant in the G2. On the other hand, the corresponding zircon Hf-isotope compositions from southwestern Laurentia almost overlap with those of the G1, especially the ~1.8 Ga zircon grains (Fig. 7a). All these signatures suggest that the KTM had a close affinity with southwestern Laurentia before ~1.65 Ga (Fig. 8a).

5.3.2. Statherian to calymmian (1.74–1.45 Ga)

Compared with the G1, the G2 sedimentary rocks contain higher proportions of ~1.75 Ga, ~2.01 Ga, and ~2.32 Ga detrial zircons (Fig. 6b), in addition to similar ~2.56 and ~1.83 Ga populations, indicating more complicated sources. Abundant ~2.56 and ~1.83 Ga detrital zircons in the G2 suggest that the KTM remained near southwestern Laurentia during 1.74–1.45 Ga. Large-scale magmatic accretionary belts, such as the 1.8–1.7 Ga Yavapai and 1.7–1.6 Ga Mazatzal belts, formed along the present-day southern flank of North America (Betts et al., 2008; Holland et al., 2015). Coeval felsic and mafic magmatism occurred in the Mawson Continent (Fig. 6b; Goodge et al., 2017; Belousova et al., 2009). These igneous rocks have a large range in zircon εHf(t) (Holland et al., 2018; Belousova et al., 2009), similar to those of the G2 (Fig. 7b).The SWEAT model shows a spatial connection between the southwest United States and East Antarctica at *ca* 1.6–1.3 Ga (Mulder et al., 2015), which has been confirmed by recent paleomagnetic data (Kirscher et al., 2021). Thus, integration of zircon age spectra

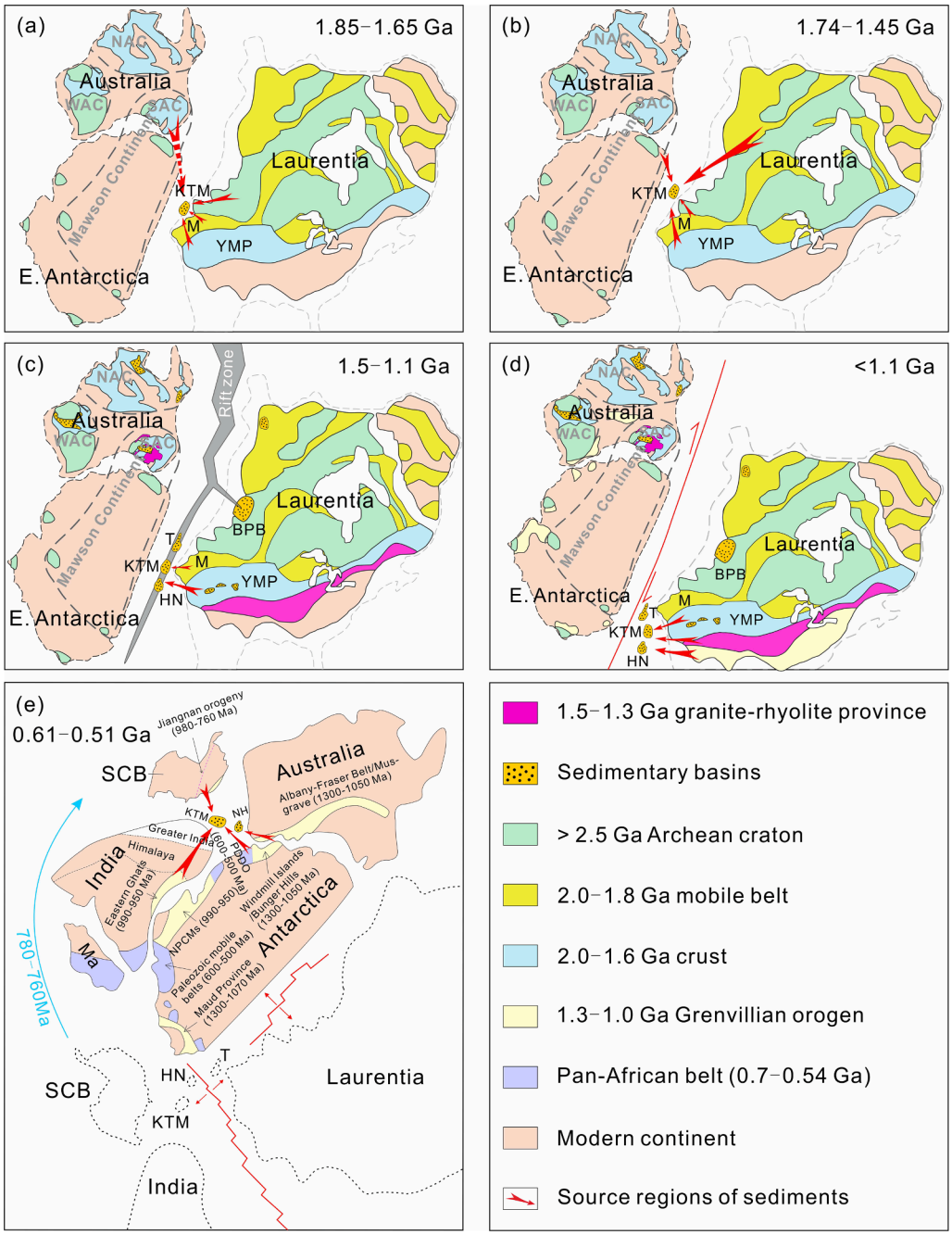

Fig. 8. Paleogeographic reconstruction showing correlations of the Kontum Massif (Central Vietnam) with East Antarctica, Australia, Laurentia, and Hainan Island from the Columbia to Gondwana supercontinents (modified from Xu et al., 2020; Goodge et al., 2017; Mulder et al., 2015, 2018; Yao et al., 2017; Belousova et al., 2009; Yu et al., 2008; Jing et al., 2021). The KTM was closely linked with the southwestern Laurentia for about billion years (a-d), and rapidly moved from the southwestern flank of Laurentia to the northern margin of East Gondwana together with South China Block in the middle Neoproterozoic (e). KTM–Kontum Massif; M–Mojave; YMP–Yavapai-Mazatzal provinces; T–Tasmania; HN–Hainan Island; BPB–Belt-Purcelt Basin; WAC–Western Australia Craton; SAC–Southern Australia Craton; NAC–Northern Australia Craton; SCB–South China Block; NPCMs–Northern Prince Charles Mountains; PDDO–Prydz-Denman-Darling orogeny; Ma–Madagascar.

with Hf-isotope compositions suggests that ~1.75 Ga detritus in the KTM were probably derived from the Yavapai-Mazatzal Belt and the Mawson Continent. The ~2.0 Ga magmatism has also been identified in East Antarctica (Belousova et al., 2009; Goodge et al., 2017). The rocks are predominantly granitoids with negative zircon εHf(t) values (Belousova et al., 2009), matching the coeval detrital zircons from the G2 (Fig. 7b). The striking peak at ~2.32 Ga in the G2 is unconspicuous in other continents (Fig. 6b), but synchronous with the 2.5–2.3 Ga Arrowsmith orogeny along the western flank of the Rae Craton in northern Laurentia (Berman et al., 2013). Furthermore, the ~2.32 Ga detrital zircons and igneous rocks in the Arrowsmith orogeny show dominantly low εHf(t) of −12.6 to −1.5 (Cui et al., 2019), overlapping those in the G2, indicating that the Arrowsmith orogen is a possible source. Consequently, the KTM may have received sediments from the Mawson Continent and the Arrowsmith orogen in addition to southwestern Laurentia during deposition of the G2 (Fig. 8b).

5.3.3. Calymmian to Ectasian (1.5–1.1 Ga)

One of the most important characteristics of the Mesoproterozoic geology is widespread continental rifting and anorogenic magmatism, following the breakup of Columbia (1.5–1.4 Ga; Tang et al., 2021). The G3 sedimentary rocks in the KTM were deposited during 1.5–1.1 Ga, synchronous with the Ewenling Formation of the Baoban complex (1.45–1.30 Ga) in Hainan Island of South China, the lower-middle Rocky Cape Group (1.45–1.33 Ga) in Tasmania, and the Belt-Purcell Supergroup (1.47–1.40 Ga) and Marquenas Formation (1.47–1.45 Ga) in southwestern Laurentia (Mulder et al., 2015; Stewart et al., 2010; Xu et al., 2020).

The age spectrum of detrital zircons in the G3 has a major peak at 1721 Ma and a minor peak at 1441 Ma with fewer ~2.57 Ga ages (Fig. 6c). Strong ~1.45 Ga bimodal magmatism has been identified in southwestern Laurentia, the KTM, and Hainan Island (Bickford et al., 2015; Zhang et al., 2018; Wang et al., 2020; Xu et al., 2020; Nakano

et al., 2021). The coeval sedimentary sequences from southwestern Laurentia and Hainan Island show similar clastic components to the G3 (Fig. 6c). Moreover, their zircon Hf-isotope compositions overlap (Fig. 7c), suggesting the same provenance. The ~1.72 Ga detrital zircons in the G3 have a larger εHf(t) range (Fig. 7c). Holland et al. (2015) reported that the Mojave and Yavapai crustal provinces respectively contain both evolved and juvenile late Paleoproterozoic crust, implying that the KTM was located near these two provinces. Therefore, the KTM together with Hainan Island probably remained connected with southwestern Laurentia during the G3 period (Fig. 8c).

The equivalent successions in Tasmania also exhibit an age spectrum and Hf-isotope compositions comparable with the G3 sedimentary rocks (Fig. 6c, 7c). Mulder et al. (2015) thought that Tasmania was situated in southwestern Laurentia and recorded a East Antarctica - Laurentia connection. Consequently, Tasmania may have been adjacent to the KTM (Fig. 8c).

5.3.4. Stenian-Tonian (< 1.1 Ga)

This period witnessed the assembly and breakup of the Rodinia supercontinent. The assembly of different continents took place along the Grenville-age orogenic belts during 1.3–0.9 Ga. The Grenvillian orogens are subdivided into the older (1300–1050 Ma) and younger (1050–900 Ma) ones. The former is distributed across southern Laurentia, western Australia, western East Antarctica, and Kalahari (Goodge et al., 2017; Fitzsimons, 2003; Kirkland et al., 2011; Möller et al., 2002; Milidragovic et al., 2011), and the latter occurs in northern East Antarctica (Mikhalsky et al., 2010, 2013) and eastern India (Chattopadhyay et al., 2015; Dasgupta et al., 2013). The G4 sedimentary rocks in the KTM have striking detrital-zircon age peaks at 1740 Ma and 1348 Ma with a minor peak at 1116 Ma. The presence of older Grenvillian detrital zircons in the G4 suggests that the KTM was close to either southern Laurentia or western Australia during their depositional time. However, the synchronous sequences in western Australia contain few late Paleoproterozoic and early Mesoproterozoic zircons (Fig. 6d), suggesting that the KTM was not close to western Australia. On the contrary, the large proportions of ~1.74 Ga and ~1.35 Ga zircons correspond to the Yavapai-Mazatzal magmatic belt and Granite-Rhyolite province in southwestern Laurentia. As stated above, the 1.8–1.6 Ga Yavapai-Mazatzal magmatic belt is a large-scale accretionary belt with mafic and felsic rocks showing varying zircon Hf-isotope compositions (Holland et al., 2015, 2018). The detrital zircons of ~1.74 Ga and ~1.35 Ga in the G4 have Hf-isotope compositions very similar to these igneous rocks in southwestern Laurentia. A weak age peak of ~1.45 Ga in the G4 is synchronous with the bimodal magmatism in the KTM, Hainan Island, and southwestern Laurentia (Xu et al., 2020; Nakano et al., 2021; Bickford et al., 2015; Wang et al., 2020). All these observations suggest that the KTM probably was still connected with southwestern Laurentia. However, coeval sedimentary rocks in southwestern Laurentia show a prominent 1250 Ma peak, which is lacking in the G4 (Fig. 6d). This suggests that the KTM might have been far from the 1250 Ma source.

The equivalent metasedimentary rocks from Hainan Island and Tasmania have detrital- zircon age spectra similar to the G4 (Fig. 6d), and their zircon Hf-isotope compositions are consistent (Fig. 7d). Mulder et al. (2018) and Yao et al. (2017) concluded that Tasmania and Hainan Island were close to southwestern Laurentia in the late Mesoproterozoic to early Neoproterozoic. Hainan Island and the KTM were also subject to the same tectonic setting during this period (Yao et al., 2017; Wang et al., 2020). Collectively, the KTM probably had a close affinity with Hainan Island, Tasmania, and southwestern Laurentia in the period of < 1.1 Ga (Fig. 8d).

5.3.5. Ediacaran (0.61–0.51 Ga)

The G5 sedimentary rocks in the KTM contain adundant Mesoproterozoic to Neoproterozoic detritus with a steep Grenvillian age peak (Fig. 6e), much different from those of the G1 to G4 sedimentary rocks, implying a drastic change in the depositional environment and provenances from the G1-4 to the G5. The significant Grenvillian detritus in the G5 suggests that the KTM was close to a Grenvillian orogenic belt during the G5 deposition. The Grenville Orogen in southern Laurentia may be a potential source for older Grenvillian detritus in the G5. However, the abundant younger Grenvillian and middle Neoproterozoic detritus is incompatible with this source (Fig. 6e). The wide spread of Grenvillian ages of detrital zircons in the G5 sedimentary rocks suggests that the KTM was located near both older and younger Grenvillian orogenic belts. Previous studies placed the Indochina Block on the northern margin of East Gondwana, adjacent to South China (Burrett et al., 2014; Cawood et al., 2018; Metcalfe, 2021). Thus, the KTM was most likely located among the Eastern Ghats Province in eastern India (Dasgupta et al., 2013), Northern Prince Charles Mountains of East Antarctica (Daczko et al., 2018), the Albany-Fraser belt and the Musgrave block in western to central Australia (Ksienzyk et al., 2012), and the Windmill Islands-Bunger Hills (Goodge et al., 2017) of East Antarctica (Fig. 8e). Weak 1434 Ma, 1749 Ma and Neoproterozoic age peaks are also consistent with those sedimentary rocks in northeastern India and western Australia (Fig. 6e). Hf-isotope compositions of these detrital zircons in the G5 match well with those from the Albany-Fraser collisional belt and northeastern India (Fig. 7e). All similarities support the KTM configuration in the northern margin of East Gondwana (Fig. 8e).

Detrital zircon ages and Hf-isotopes and paleomagnetic data indicate that South China was between western Australia and northeastern India during latest Ediacaran and early Cambrian time (Yu et al., 2008; Zhang et al., 2015; Wang et al., 2021; Xue et al., 2021). The G5 sedimentary rocks have detrital zircon age spectra similar to those Ediacaran sedimentary rocks from the West Cathaysia Block (Fig. 6e), but different from those of the West Yangtze Block. Moreover, their zircon Hf-isotope compositions are also similar to those of the West Cathaysia Block but different from those of West Yangtze Block (Fig. 7e). These lines of evidence imply that the KTM (Indochina) was situated on the southwest flank of South China and closer to northeastern India and western Australia (Fig. 8e), consistent with previous reconstruction models (Wang et al., 2016b).

The above discussions suggest that the KTM experienced rapid movement from the core of Rodinia (near southwestern Laurentia) to the northern margin of East Gondwana (near eastern India - South China) from the G4 to the G5. This is a remarkable drift, and paleomagnetic data seem to support it (Jing et al., 2021). Based on the new paleomagnetic data obtained from the Tonian Lower Liantuo Formation in central South China and other available data, Jing et al. (2021) suggest that the South China Block and India craton were located near southwestern Laurentia at *ca* 800 Ma, and moved rapidly to the Northern Hemisphere from 800 Ma to 760 Ma (Jing et al., 2021). The KTM shows an affinity with South China and eastern India during the G5, and was situated near southwestern Laurentia during the G4, which is consistent with the positions of South China and India. Therefore, the KTM together with South China and India probably quickly drifted to the Northern Hemisphere from the G4 to the G5 periods (Fig. 8e). Drastic changes of clastic components and provenances between the G4 and G5 sedimentary rocks support this model.

6. Conclusions

The basement rocks of the KTM consist mainly of different periods of Precambrian sedimentary rocks and lesser Mesoproterozoic igneous rocks. These sedimentary rocks were deposited in five periods, 1.85–1.65 Ga, 1.74–1.45 Ga, 1.4–1.1 Ga, 1.1–0.81 Ga, and 0.61–0.51 Ga, labeled as G1 to G5. Late Paleoproterozoic (G1) metasedimentary rocks are the oldest lithological unit identified in the KTM to date. The G1 and G2 sedimentary rocks are composed mainly of late Neoarchean and late Paleoproterozoic detritus, and the G3 and G4 sedimentary rocks comprise abundant late Paleoproterozoic and middle Mesoproterozoic ones. The G5 sedimentary rocks contain dominantly Mesoproterozoic

detrital zircons with an age peak at 1.06–1.01 Ga, much different from the G4, suggesting a abrupt change in the deposition environment and provenance from the G4 to the G5. Few Precambrian igneous rocks are recognized in the KTM, except ~1.45 Ga igneous rocks, suggesting that the most Precambrian detritus in the G1 to G5 sedimentary rocks are exotic. Comprehensive comparisons of the age spectra and Hf-isotope compositions of detrital zircons in these sedimentary rocks with magmatic events and detrital zircons from synchronous successions in different continents and microcontinents suggest that the KTM retained a long connection with southwestern Laurentia from the G1 to the G4 (1.8 Ga to 0.8 Ga), and near Mawson, Hainan Island and Tasmania at least from the G3 to the G4. Subsequently, the KTM was situated at the northern margin of East Gondwana during the G5 deposition. The KTM, with South China, India and Hainan Island, experienced rapid northward drift from the G4 to the G5. This finding is consistent with paleomagnetic data and the drastic change in the clastic components between the G4 and the G5 sedimentary units.

CRediT authorship contribution statement

Wei Jiang: Writing – original draft, Data curation. **Jin-Hai Yu:** Conceptualization, Supervision, Project administration. **W.L. Griffin:** Writing – review & editing. **Fangqian Wang:** Data curation. **Xiaolei Wang:** Formal analysis, Writing – review & editing. **TrungHieu Pham:** Investigation. **DinhLuyen Nguyen:** Investigation.

Declaration of Competing Interest

The authors declare that they have no known competing financial interests or personal relationships that could have appeared to influence the work reported in this paper.

Acknowledgments

This work was supported by the National Natural Science Foundation of China (grant no. 41772053). We thank Dr. Tao Yang and Mr. Bing Wu for their assistance in zircon Hf–isotope analysis and U–Pb dating at Nanjing University. This is contribution XXX from the ARC Centre of Excellence for Core to Crust Fluid Systems (www.ccfs.mq.edu.au) and XXX from the GEMOC Key Centre (www.gemoc.mq.edu.au).

Appendix A. Supplementary material

Supplementary data to this article can be found online at https://doi.org/10.1016/j.precamres.2022.106725.

References

Andersen, T., 2002. Correction of common lead in U-Pb analyses that do not report 204Pb. Chem. Geol. 192, 59–79. https://doi.org/10.1016/s0009-2541(02)00195-x.

Belousova, E.A., Reid, A.J., Griffin, W.L., O'Reilly, S.Y., 2009. Rejuvenation vs. recycling of Archean crust in the Gawler Craton, South Australia: Evidence from U-Pb and Hf isotopes in detrital zircon. Lithos 113 (3–4), 570–582. https://doi.org/10.1016/j.lithos.2009.06.028.

Berman, R.G., Pehrsson, S., Davis, W.J., Ryan, J.J., Qui, H., Ashton, K.E., 2013. The Arrowsmith orogeny: geochronological and thermobarometric constraintson its extent and tectonic setting in the Rae craton, with implications forpre-Nuna supercontinent reconstruction. Precambrian Res. 232, 44–69. https://doi.org/10.1016/j.precamres.2012.10.015.

Betts, P.G., Giles, D., Schaefer, B.F., 2008. Comparing 1800–1600 Ma accretionary and basin processes in Australia and Laurentia: possible geographic connections in Columbia. Precambrian Res. 166, 81–92. https://doi.org/10.1016/j.precamres.2007.03.007.

Blichert-Toft, J., Albarede, F., 1997. The Lu-Hf isotope geochemistry of chondrites and the evolution of the mantle-crust system. Earth Planet. Sci. Lett. 148, 243–258. https://doi.org/10.1016/s0012-821x(97)00198-2.

Bickford, M.E., Van Schmus, W.R., Karlstrom, K.E., Mueller, P.A., Kamenov, G.D., 2015. Mesoproterozoic-trans-Laurentian magmatism: A synthesis of continent-wide age distributions, new SIMS U-Pb ages, zircon saturation temperatures, and Hf and Nd isotopic compositions. Precambrian Res. 265, 286–312. https://doi.org/10.1016/j.precamres.2014.11.024.

Boher, M., Abouchami, W., Michard, A., Albarede, F., Arndt, N.T., 1992. Crustal growth in west Africa at 2.1 Ga. J. Geophys. Res. Solid Earth 97 (B1), 345–369. https://doi.org/10.1029/91jb01640.

Breemen, O., Harper, C.T., Berman, R.G., Wodicka, N., 2007. Crustal evolution and Neoarchean assembly of the central-southern Hearne domains: Evidence from U-Pb geochronology and Sm-Nd isotopes of the Phelps Lake area, northeastern Saskatchewan. Precambrian Res. 159, 33–59. https://doi.org/10.1016/j.precamres.2007.04.014.

Bui, V.T.S., Osanai, Y., Nakano, N., Adachi, T., Kitano, I., Owada, M., 2020. Timing of high-grade metamorphism in the Kontum Massif, Vietnam: Constraints from zircon-monazite multi-geochronology and trace elements geochemistry of zircon-monazite-garnet. J. Asian Earth Sci. 187, 104084 https://doi.org/10.1016/j.jseaes.2019.104084.

Burrett, C., Zaw, K., Meffre, S., Lai, C.K., Khositanont, S., Chaodumrong, P., Udchachon, M., Ekins, S., Halpin, J., 2014. The configuration of Greater Gondwana-evidence from LAICPMS, U-Pb geochronology of detrital zircons from the Palaeozoic and Mesozoic of Southeast Asia and China. Gondwana Res. 26 (1), 31–51. https://doi.org/10.1016/j.gr.2013.05.020.

Cawood, P.A., Zhao, G., Yao, J., Wang, W., Xu, Y., Wang, Y., 2018. Reconstructing South China in phanerozoic and precambrian supercontinents. Earth Sci. Rev. 186, 173–194. https://doi.org/10.1016/j.earscirev.2017.06.001.

Chattopadhyay, S., Upadhyay, D., Nanda, J.K., Mezger, K., Pruseth, K.L., Berndt, J., 2015. Proto-India was a part of Rodinia: Evidence from Grenville-age suturing of the Eastern Ghats Province with the Paleoarchean Singhbhum Craton. Precambrian Res. 266, 506–529. https://doi.org/10.1016/j.precamres.2015.05.030.

Cui, X.Z., Wang, J., Sun, Z.M., Wang, W., Deng, Q., Ren, G.M., Liao, S.Y., Huang, M.D., Chen, F.L., Ren, F., 2019. Early Paleoproterozoic (ca. 2.36 Ga) post-collisional granitoids in Yunnan, SW China: Implications for linkage between Yangtze and Laurentia in the Columbia supercontinent. J. Asian Earth Sci. 169, 308–322. https://doi.org/10.1016/j.jseaes.2018.10.026.

Daczko, N.R., Halpin, J.A., Fitzsimons, I.C.W., Whittaker, J.M., 2018. A cryptic Gondwana-forming orogen located in Antarctica. Sci. Rep. 8 (1), 8371. https://doi.org/10.1038/s41598-018-26530-1.

Dasgupta, S., Bose, S., Das, K., 2013. Tectonic evolution of the Eastern Ghats Belt, India. Precambrian Res. 227, 247–258. https://doi.org/10.1016/j.precamres.2012.04.005.

Davis, W.J., Hanmer, S., Tella, S., Sandeman, H., Ryan, J.J., 2006. U-Pb Geochronology of the MacQuoid supracrustal belt and Cross Bay plutonic complex: key components of the northwestern Hearne subdomain, Western Churchill Province, Nunavut, Canada. Precambrian Res. 145, 53–80. https://doi.org/10.1016/j.precamres.2005.11.016.

Evans, D.A., Mitchell, R.N., 2011. Assembly and breakup of the core of Paleoproterozoic-Mesoproterozoic supercontinent Nuna. Geology 39, 443–446. https://doi.org/10.1130/g31654.1.

Faure, M., Nguyen, V.V., Hoai, L.T.T., Lepvrier, C., 2018. Early Paleozoic or Early-Middle Triassic collision between the South China and Indochina Blocks: The controversy resolved? Structural insights from the Kon Tum massif (Central Vietnam). J. Asian Earth Sci. 166, 162–180. https://doi.org/10.1016/j.jseaes.2018.07.015.

Fitzsimons, I.C.W., 2003. Proterozoic basement provinces of southern and southwestern Australia, and their correlation with Antarctica. Proterozoic East Gondwana: supercontinent assembly and breakup. Geol. Soc. London, Special Publ. 206, 93–130. https://doi.org/10.1144/gsl.sp.2003.206.01.07.

Furlanetto, F., Thorkelson, D.J., Rainbird, R.H., Davis, W.J., Gibson, H.D., Marshall, D. D., 2016. The Paleoproterozoic Wernecke Supergroup of Yukon, Canada: Relationships to orogeny in northwestern Laurentia and basins in North America, East Australia, and China. Gondwana Res. 39, 14–40. https://doi.org/10.1016/j.gr.2016.06.007.

Gardiner, N.J., Kirkland, C.L., Hollis, J., Szilas, K., Steenfelt, A., Yakymchuk, C., Heide-Jørgensen, H., 2019. Building mesoarchaean crust upon Eoarchaean roots: the Akia terrane, West Greenland. Contrib. Mineral. Petrol. 174 (3), 1–19. https://doi.org/10.1007/s00410-019-1554-x.

Goodge, J.W., Fanning, C.M., Fisher, C.M., Vervoort, J.D., 2017. Proterozoic crustal evolution of central East Antarctica: Age and isotopic evidence from glacial igneous clasts, and links with Australia and Laurentia. Precambrian Res. 299, 151–176. https://doi.org/10.1016/j.precamres.2017.07.026.

Griffin, W.L., Wang, X., Jackson, S.E., Pearson, N.J., O'Reilly, S.Y., Xu, X.S., Zhou, X.M., 2002. Zircon chemistry and magma mixing, SE China: in-situ analysis of Hf isotopes, Tonglu and Pingtan igneous complexes. Lithos 61, 237–269. https://doi.org/10.1016/s0024-4937(02)00082-8.

Griffin, W.L., Powell, W.J., Pearson, N.J., O'Reilly, S.Y., 2008. GLITTER: data reduction software for laser ablation ICP-MS. Laser Ablation-ICP-MS in the Earth Sciences. Mineral. Assoc. Canada Short Course Series 40, 204–207.

Griffin, W.L., Belousova, E.A., Shee, S.R., Pearson, N.J., O'Reilly, S.Y., 2004. Archaean crustal evolution in the northern Yilgarn Craton: U-Pb and Hf-isotope evidence from detrital zircons. Precambrian Res. 131, 231–282. https://doi.org/10.1016/j.precamres.2003.12.011.

Grochowski, J., Kuchenbecker, M., Barbuena, D., Novo, T., 2021. Disclosing Rhyacian/Orosirian orogenic magmatism within the Guanhães basement inlier, Araçuaí Orogen, Brazil: A new piece on the assembly of the São Francisco-Congo paleocontinent. Precambrian Res. 363, 106329 https://doi.org/10.1016/j.precamres.2021.106329.

Hand, M., Reid, A., Jagodzinski, E., 2007. Tectonic framework and evolution of the Gawler Craton, Southern Australia. Econ. Geol. 102, 1377–1395. https://doi.org/10.2113/gsecongeo.102.8.1377.

Holland, M.E., Karlstrom, K.E., Doe, M.F., Gehrels, G.E., Pecha, M., Shufeldt, O.P., Begg, G., Griffin, W.L., Belousova, E., 2015. An imbricate midcrustal suture zone:

The Mojave-Yavapai Province boundary in Grand Canyon, Arizona. Geol. Soc. Am. Bull. 127 (9–10), 1391–1410. https://doi.org/10.1130/b31232.1.
Holland, M.E., Karlstrom, K.E., Gehrels, G., Shufeldt, O.P., Begg, G., Griffin, W., Belousova, E., 2018. The Paleoproterozoic Vishnu basin in southwestern Laurentia: implications for supercontinent reconstructions, crustal growth, and the origin of the Mojave crustal province. Precambrian Res. 308, 1–17. https://doi.org/10.1016/j.precamres.2018.02.001.
Howard, K.E., Hand, M., Barovich, K.M., Reid, A., Wade, B.P., Belousova, E.A., 2009. Detrital zircon ages: improving interpretation via Nd and Hf isotopic data. Chem. Geol. 262, 277–292. https://doi.org/10.1016/j.chemgeo.2009.01.029.
Hutchison, C.S., 1989. Geological Evolution of Southeast Asia. Clarendon, Oxford, p. 368.
Iaccheri, L.M., Bagas, L., 2020. Zircon provenances provide paleogeographic constraints on models reconstructing the Paleoproterozoic Columbia Supercontinent. Gondwana Res. 82, 254–266. https://doi.org/10.1016/j.gr.2020.01.008.
Jiang, W., Yu, J.H., Wang, X.L., Griffin, W.L., Pham, T.H., Nguyen, D.L., Wang, F.Q., 2020. Early Paleozoic magmatism in northern Kontum Massif, Central Vietnam: Insights into tectonic evolution of the eastern Indochina Block. Lithos 376–377, 105750. https://doi.org/10.1016/j.lithos.2020.105750.
Jing, X., Evans, D.A., Yang, Z., Tong, Y., Xu, Y., Wang, H., 2021. Inverted South China: A novel configuration for Rodinia and its breakup. Geology 49 (4), 463–467. https://doi.org/10.1130/geol.s.13262831.v1.
Johnson, S.P., Sheppard, S., Rasmussen, B., Wingate, M.T.D., Kirkland, C.L., Muhling, J. R., Fletcher, I.R., Belousova, E.A., 2011. Two collisions, two sutures: punctuated pre-1950 Ma assembly of the West Australian Craton during the Ophthalmian and Glenburgh Orogenies. Precambrian Res. 189, 239–262. https://doi.org/10.1016/j.precamres.2011.07.011.
Kaur, P., Chaudhri, N., Raczek, I., Kröner, A., Hofmann, A., 2009. Record of 1.82 Ga Andean-type continental arc magmatism in NE Rajasthan, India: Insights from zircon and Sm-Nd ages, combined with Nd-Sr isotope geochemistry. Gondwana Res. 16 (1), 56–71. https://doi.org/10.1016/j.gr.2009.03.009.
Kaur, P., Zeh, A., Chaudhri, N., 2017. Palaeoproterozoic continental arc magmatism, and Neoproterozoic metamorphism in the Aravalli-Delhi orogenic belt, NW India: New constraints from in situ zircon U-Pb-Hf isotope systematics, monazite dating and wholerock geochemistry. J. Asian Earth Sci. 136, 68–88. https://doi.org/10.1016/j.jseaes.2017.01.024.
Kirkland, C.L., Spaggiari, C.V., Pawley, M.J., Wingate, M.T.D., Smithies, R.H., Howard, M.H., Tyler, I.M., Belousova, E., Poujol, M., 2011. On the edge: U-Pb, Lu-Hf, and Sm-Nd data suggests reworking of the Yilgarn craton margin during formation of the Albany-Fraser Orogen. Precambrian Res. 187, 223–247. https://doi.org/10.1016/j.precamres.2011.03.002.
Kirscher, U., Mitchell, R.N., Liu, Y., Nordsvan, A.R., Cox, G.M., Pisarevsky, S.A., Wang, C., Wu, L., Murphy, J.B., Li, Z.X., 2021. Paleomagnetic constraints on the duration of the Australia-Laurentia connection in the core of the Nuna supercontinent. Geology 49 (2), 174–179. https://doi.org/10.1130/geol.s.12935030.v1.
Ksienzyk, A.K., Jacobs, J., Boger, S., Kosler, J., Sircombe, K.N., Whitehouse, M.J., 2012. U-Pb ages of metamorphic monazite and detrital zircon from the Northampton Complex: evidence of two orogenic cycles in Western Australia. Precambrian Res. 198–199, 37–50. https://doi.org/10.1016/j.precamres.2011.12.011.
Lan, C.Y., Chung, S.L., Van Long, T., Lo, C.H., Lee, T.Y., Mertzman, S.A., Shen, J., 2003. Geochemical and Sr-Nd isotopic constraints from the Kontum massif, central Vietnam on the crustal evolution of the Indochina block. Precambrian Res. 122, 7–27. https://doi.org/10.1016/s0301-9268(02)00205-x.
Lepvrier, C., Nguyen, V.V., Maluski, H., Phan, T.T., Tich, V.V., 2008. Indosinian tectonics in Vietnam. Compt. Rendus Geosci. 340 (2–3), 94–111. https://doi.org/10.1016/j.crte.2007.10.005.
Ludwig, K., 2003. Isoplot/ex Version 3: A Geochronological Toolkit for Microsoft Excel. Geochronology Center, Berkeley.
Maluski, H., Lepvrier, C., Leyreloup, A., Tich, V., Thi, P., 2005. 40Ar–39Ar geochronology of the charnockites and granulites of the Kannack complex, Kon Tum Massif, Vietnam. J. Asian Earth Sci. 25, 653–677.
Metcalfe, I., 2021. Multiple Tethyan ocean basins and orogenic belts in Asia. Gondwana Res. 100, 87–130. https://doi.org/10.1016/j.gr.2021.01.012.
Mikhalsky, E.V., Henjes-Kunst, F., Belyatsky, B.V., Roland, N.W., Sergeev, S.A., 2010. New Sm-Nd, Rb-Sr, U-Pb and Hf isotope systematics for the southern Prince Charles Mountains (East Antarctica) and its tectonic implications. Precambrian Res. 182, 101–123. https://doi.org/10.1016/j.precamres.2010.07.004.
Mikhalsky, E.V., Sheraton, J.W., Kudriavtsev, I.V., Sergeev, S.A., Kovach, V.P., Kamenev, I.A., Laiba, A.A., 2013. The Mesoproterozoic Rayner Province in the Lambert Glacier area: its age, origin, isotopic structure and implications for Australia-Antarctica correlations. Antarctica and Supercontinent Evolution. Geol. Soc. London, Special Publ. 383, 35–57. https://doi.org/10.1144/sp383.1.
Milidragovic, D., Thorkelson, D.J., Davis, W.J., Marshall1, D.D., Gibson, H.D., 2011. Evidence for late Mesoproterozoic tectonism in northern Yukon and the identification of a Grenville-age tectonothermal belt in western Laurentia. Terra Nova, 23, 307–313. https://doi.org/10.1111/j.1365-3121.2011.01015.x.
Möller, A., Post, N.J., Hensen, B.J., 2002. Crustal residence history and garnet Sm-Nd ages of high-grade metamorphic rocks from the Windmill Islands area, East Antarctica. Int. J. Earth Sci. 91, 993–1004. https://doi.org/10.1007/s00531-002-0291-x.
Mulder, J.A., Halpin, J.A., Daczko, N.R., 2015. Mesoproterozoic Tasmania: Witness to the East Antarctica-Laurentia connection within Nuna. Geology 43, 759–762. https://doi.org/10.1130/g36850.1.
Mulder, J.A., Karlstrom, K.E., Halpin, J.A., Merdith, A.S., Spencer, C.J., Berry, R.F., McDonald, B., 2018. Rodinian devil in disguise: Correlation of 1.25–1.10 Ga strata between Tasmania and Grand Canyon. Geology 46 (11), 991–994. https://doi.org/10.1130/g45225.1.
Mueller, P.A., Frost, C.D., 2006. The Wyoming Province: a distinctive Archean craton in Laurentian North America. Can. J. Earth Sci. 43 (10), 1391–1397. https://doi.org/10.1139/e06-075.
Mueller, P.A., Wooden, J.L., Mogk, D.W., Foster, D.A., 2011. Paleoproterozoic evolution of the Farmington zone: Implications for terrane accretion in southwestern Laurentia. Lithosphere 3 (6), 401–408. https://doi.org/10.1130/l161.1.
Nakano, N., Osanai, Y., Owada, M., Binh, P., Hokada, T., Kaiden, H., Bui, V.T.S., 2021. Evolution of the Indochina block from its formation to amalgamation with Asia: Constraints from protoliths in the Kontum Massif, Vietnam. Gondwana Res. 90, 47–62. https://doi.org/10.1016/j.gr.2020.11.002.
Nakano, N., Osanai, Y., Owada, M., Nam, T.N., Charusiri, P., Khamphavong, K., 2013. Tectonic evolution of high-grade metamorphic terranes in central Vietnam: Constraints from large-scale monazite geochronology. J. Asian Earth Sci. 73, 520–539. https://doi.org/10.1016/j.jseaes.2013.05.010.
Nguyen, Q.M., Feng, Q.H., Zi, J.W., Zhao, T.Y., Tran, H.T., Ngo, T.X., Tran, D.M., Nguyen, H.Q., 2019. Cambrian intra-oceanic arc trondhjemite and tonalite in the Tam Ky-Phuoc Son Suture Zone, central Vietnam: Implications for the early Paleozoic assembly of the Indochina Block. Gondwana Res. 70, 151–170. https://doi.org/10.1016/j.gr.2019.01.002.
Osanai, Y., Nakano, N., Owada, M., Tran, N.N., Toyoshima, T., Tsunogae, T., Pham, B., 2004. Permo-Triassic ultrahigh-temperature metamorphism in the Kontum massif, central Vietnam. J. Mineral. Petrol. Sci. 99 (4), 225–241.
Partin, C., Bekker, A., Sylvester, P., Wodicka, N., Stern, R., Chacko, T., Heaman, L., 2014. Filling in the juvenile magmatic gap: evidence for uninterrupted Paleoprotero-zoic plate tectonics. Earth Planet. Sci. Lett. 388, 123–133. https://doi.org/10.1016/j.epsl.2013.11.041.
Reid, A.J., Jagodzinski, E.A., Armit, R.J., Dutch, R.A., Kirkland, C.L., Betts, P.G., Schaefer, B.F., 2014. U-Pb and Hf isotopic evidence for Neoarchean and Paleoproterozoic basement in the buried northern Gawler Craton, South Australia. Precambrian Res. 250, 127–142. https://doi.org/10.1016/j.precamres.2014.05.019.
Richards, A., Argles, T., Harris, N., Parrish, R., Ahmad, T., Darbyshire, F., Draganits, E., 2005. Himalayan architecture constrained by isotopic tracers from clastic sediments. Earth Planet. Sci. Lett. 236, 773–796. https://doi.org/10.1016/j.epsl.2005.05.034.
Rosing, M.T., Nutman, A.P., Løfqvist, L., 2001. A new fragment of the early earth crust: the Aasivik terrane of West Greenland. Precambrian Res. 105 (2–4), 115–128. https://doi.org/10.1016/s0301-9268(00)00107-8.
Scherer, E., Munker, C., Mezger, K., 2001. Calibration of the lutetium-hafnium clock. Science 293, 683–687. https://doi.org/10.1126/science.1061372.
Schneider, D.A., Heizler, M.T., Bickford, M.E., Wortman, G.L., Condie, K.C., Perilli, S., 2007. Timing constraints of orogeny to cratonization: Thermochronology of the Paleoproterozoic Trans-Hudson orogen, Manitoba and Saskatchewan, Canada. Precambrian Res. 153, 65–95. https://doi.org/10.1016/j.precamres.2006.11.007.
Sen, A., Sen, K., Srivastava, H.B., Singhal, S., Phukon, P., 2019. Age and geochemistry of the Paleoproterozoic Bhatwari Gneiss of Garhwal Lesser Himalaya, NW India: implications for the pre-Himalayan magmatic history of the Lesser Himalayan basement rocks. Geol. Soc. Spec. Publ. 481 (1), 319–339. https://doi.org/10.1144/sp481.6.
Stewart, E.D., Link, P.K., Fanning, C.M., Frost, C.D., McCurry, M., 2010. Paleogeographic implications of non-North American sediment in the Mesoproterozoic upper Belt Supergroup and Lemhi Group, Idaho and Montana, USA. Geology 38 (10), 927–930. https://doi.org/10.1130/g31194.1.
Swain, G., Woodhouse, A., Hand, M., Barovich, K., Schwarz, M., Fanning, C.M., 2005. Provenance and tectonic development of the late Archaean Gawler Craton, Australia: U-Pb zircon, geochemical and Sm-Nd isotopic implications. Precambrian Res. 141, 106–136. https://doi.org/10.1016/j.precamres.2005.08.004.
Tang, L., Santosh, M., 2018. Neoarchean-Paleoproterozoic terrane assembly and Wilson cycle in the North China Craton: an overview from the central segment of the Trans-North China Orogen. Earth Sci. Rev. 182, 1–27. https://doi.org/10.1016/j.earscirev.2018.04.010.
Tang, M., Chu, X., Hao, J., Shen, B., 2021. Orogenic quiescence in Earth's middle age. Science 371 (6530), 728–731. https://doi.org/10.7185/gold2021.4320.
Tran, H.T., Zaw, K., Halpin, J., Manaka, T., Meffre, S., Lai, C.K., Lee, Y., Le, H.V., Dinh, S., 2014. The Tam Ky-Phuoc Son Shear Zone in central Vietnam: tectonic and metallogenic implications. Gondwana Res. 26, 144–164. https://doi.org/10.1016/j.gr.2013.04.008.
Tran, V.T., Faure, M., Nguyen, V.V., Bui, H.H., Fyhn, M.B.W., Nguyen, T.Q., Lepvrier, C., Thomsen, T.B., Tani, K., Charusiri, P., 2020. Neoproterozoic to Early Triassic tectono-stratigraphic evolution of Indochina and adjacent areas: A review with new data. J. Asian Earth Sci. 191, 104231 https://doi.org/10.1016/j.jseaes.2020.104231.
Vervoort, J.D., Lewis, R.S., Fisher, C., Gaschnig, R.M., Jansen, A.C., Brewer, R., 2016. Neoarchean and Paleoproterozoic crystalline basement rocks of north-central Idaho: Constraints on the formation of western Laurentia. Geol. Soc. Am. Bull. 128 (1–2), 94–109. https://doi.org/10.1130/b31150.1.
Wang, C., Liang, X.Q., Foster, D.A., Fu, J.G., Jiang, Y., Dong, C.G., Zhou, Y., Wen, S., Van Quynh, P., 2016a. Detrital zircon U-Pb geochronology, Lu-Hf isotopes and REE geochemistry constrains on the provenance and tectonic setting of Indochina Block in the Paleozoic. Tectonophysics 677–678, 125–134. https://doi.org/10.1016/j.tecto.2016.04.008.
Wang, F.Q., Yu, J.H., Nguyen, D.L., Jiang, W., 2020. Precambrian Crust Components and Its Tectonic Evolution of the Kontum Massif, Central Vietnam. Geol. J. China Univ. 26 (2), 161–174 in Chinese with English abstract.
Wang, W., Cawood, P.A., Pandit, M.K., Xia, X.P., Raveggi, M., Zhao, J.H., Zheng, J.P., Qi, L., 2021. Fragmentation of South China from greater India during the Rodinia-

Gondwana transition. Geology 49 (2), 228–232. https://doi.org/10.1130/geol.s.12990911.v1.

Wang, W., Cawood, P.A., Zhou, M.F., Zhao, J.H., 2016b. Paleoproterozoic magmatic and metamorphic events link Yangtze to northwest Laurentia in the Nuna supercontinent. Earth Planet. Sci. Lett. 433, 269–279. https://doi.org/10.1016/j.epsl.2015.11.005.

Xu, Y.J., Cawood, P.A., Zhang, H.C., Zi, J.W., Zhou, J.B., Li, L.X., Du, Y.S., 2020. The Mesoproterozoic Baoban Complex, South China: A missing fragment of western Laurentian lithosphere. Geol. Soc. Am. Bull. 132 (7–8), 1404–1418. https://doi.org/10.1130/b35380.1.

Xue, E.K., Wang, W., Zhou, M.F., Pandit, M.K., Huang, S.F., Lu, G.M., 2021. Late Neoproterozoic-early Paleozoic basin evolution in the Cathaysia Block, South China: Implications of spatio-temporal provenance changes on the paleogeographic position reconstructions in supercontinent cycles. Geol. Soc. Am. Bull. 133 (3–4), 717–739. https://doi.org/10.1130/gsab.s.12613640.v1.

Yang, C.X., Santosh, M., Gao, P., Kim, S.W., Kwon, S., 2021. Late Paleoproterozoic post-collisional bimodal magmatism in the North China Craton: Insights from the Miyun gabbro-granite suite. Precambrian Res. 354, 106084 https://doi.org/10.1016/j.precamres.2020.106084.

Yang, J., Gao, S., Chen, C., Tang, Y.Y., Yuan, H.L., Gong, H.J., Xie, S.W., Wang, J.Q., 2009. Episodic crustal growth of North China as revealed by U-Pb age and Hf isotopes of detrital zircons from modern rivers. Geochim. Cosmochim. Acta. 73 (9), 2660–2673. https://doi.org/10.1016/j.gca.2009.02.007.

Yao, W.H., Li, Z.X., Li, W.X., Li, X.H., 2017. Proterozoic tectonics of Hainan Island in supercontinent cycles: New insights from geochronological and isotopic results. Precambrian Res. 290, 86–100. https://doi.org/10.1016/j.precamres.2017.01.001.

Yu, J.H., O'Reilly, S.Y., Wang, L.J., Griffin, W.L., Zhang, M., Wang, R.C., Jiang, S.Y., Shu, L.S., 2008. Where was South China in the Rodinia supercontinent? Evidence from U-Pb ages and Hf isotopes of detrital zircons. Precambrian Res. 164, 1–15. https://doi.org/10.1016/j.precamres.2008.03.002.

Yu, J.H., O'Reilly, S.Y., Wang, L., Griffin, W.L., Zhou, M.F., Zhang, M., Shu, L.S., 2010. Components and episodic growth of Precambrian crust in the Cathaysia Block, South China: Evidence from U-Pb ages and Hf isotopes of zircons in Neoproterozoic sediments. Precambr. Res. 181 (1–4), 97–114. https://doi.org/10.1016/j.precamres.2010.05.016.

Yu, J.H., O'Reilly, S.Y., Zhou, M.F., Griffin, W.L., Wang, L.J., 2012. U-Pb geochronology and Hf-Nd isotopic geochemistry of the Badu complex, south-eastern China: Implications for the Precambrian crustal evolution and paleogeography of the Cathaysia block. Precambrian Res. 222–223, 424–449. https://doi.org/10.1016/j.precamres.2011.07.014.

Yu, J.H., Wang, L.J., O'Reilly, S.Y., Griffin, W.L., Zhang, M., Li, C., Shu, L., 2009. A Paleoproterozoic orogeny recorded in a long-lived cratonic remnant (Wuyishan terrane), eastern Cathaysia Block, China. Precambrian Res. 174, 347–363. https://doi.org/10.1016/j.precamres.2009.08.009.

Yuan, H.L., Wu, F.Y., Gao, S., Liu, X.M., Xu, P., Sun, D.Y., 2003. Determination of U-Pb age and rare earth element concentrations of zircons from Cenozoic intrusions in northeastern China by laser ablation ICP-MS. Chin. Sci. Bull. 48, 2411–2421. https://doi.org/10.1360/03wd0139.

Zeh, A., Wilson, A.H., Ovtcharova, M., 2016. Source and age of upper Transvaal Supergroup, South Africa: Age-Hf isotope record of zircons in Magaliesberg quartzite and Dullstroom lava, and implications for Paleoproterozoic (2.5–2.0 Ga) continent reconstruction. Precambrian Res. 278, 1–21. https://doi.org/10.1016/j.precamres.2016.03.017.

Zhai, M.G., Hu, B., Zhao, T., Peng, P., Meng, Q., 2015. Late Paleoproterozoic-Neoproterozoic multi-rifting events in the North China Craton and their geological significance: A study advance and review. Tectonophysics 662, 153–166. https://doi.org/10.1016/j.tecto.2015.01.019.

Zhang, L., Wang, Y., Qian, X., Zhang, Y., He, H., Zhang, A., 2018. Petrogenesis of Mesoproterozoic mafic rocks in Hainan (South China) and its implication on the southwest Hainan-Laurentia-Australia connection. Precambrian Res. 313, 119–133. https://doi.org/10.1016/j.precamres.2018.05.002.

Zhang, S.H., Li, H.Y., Jiang, G.Q., Evans, D.A.D., Dong, J., Wu, H.C., Yang, T.S., Liu, P.J., Xiao, Q.S., 2015. New paleomagnetic results from the Ediacaran Doushantuo Formation in South China and their paleogeographic implications. Precambrian Res. 259, 130–142. https://doi.org/10.1016/j.precamres.2014.09.018.

Zhao, G.C., Cawood, P.A., Wilde, S.A., Sun, M., 2002. Review of global 2.1–1.8 Ga orogens: implications for a pre-Rodinia supercontinent. Earth-Sci. Rev. 59 (1–4), 125–162. https://doi.org/10.1016/j.earscirev.2004.02.003.

Zhao, G.C., Li, S.Z., Sun, M., Wilde, S.A., 2011. Assembly, accretion, and break-up of the Palaeo-Mesoproterozoic Columbia supercontinent: record in the North China Craton revisited. Int. Geol. Rev. 53 (11–12), 1331–1356. https://doi.org/10.1080/00206814.2010.527631.